Journal Pre-proofs

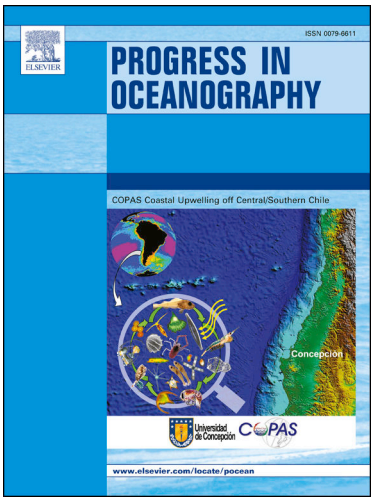

Impact of multiple drivers on the trophic position, functional diversity, and ecological memory of benthic macrofauna – analysis of 40 years of data using a complex model hierarchy

Joachim W Dippner, Ana Fernández Carrera, Ingrid Kröncke, Iris Liskow, Natalie Loick–Wilde, Maren Voss

PII: S0079-6611(25)00149-1
DOI: https://doi.org/10.1016/j.pocean.2025.103561
Reference: PROOCE 103561

To appear in: *Progress in Oceanography*

Received Date: 1 August 2024
Revised Date: 12 August 2025
Accepted Date: 25 August 2025

Please cite this article as: Dippner, J.W., Carrera, A.F., Kröncke, I., Liskow, I., Loick–Wilde, N., Voss, M., Impact of multiple drivers on the trophic position, functional diversity, and ecological memory of benthic macrofauna – analysis of 40 years of data using a complex model hierarchy, *Progress in Oceanography* (2025), doi: https://doi.org/10.1016/j.pocean.2025.103561

Impact of Multiple Drivers on the Trophic Position, Functional Diversity, and Ecological Memory of Benthic Macrofauna – Analysis of 40 Years of Data Using a Complex Model Hierarchy

Joachim W Dippner[1*], Ana Fernández Carrera[2], Ingrid Kröncke[3,4], Iris Liskow[1], Natalie Loick–Wilde[1], Maren Voss[1]

[1] Leibniz Institute for Baltic Sea Research Warnemünde, Rostock

[2] Institute of Oceanography and Global Change, University of Las Palmas de Gran Canaria

[3] Senckenberg am Meer, Department of Marine Research, Wilhelmshaven

[4] Institute for Chemistry and Biology of the marine Environment, Carl von Ossietzky University, Oldenburg

*corresponding author:

Joachim W. Dippner

Leibniz Institute for Baltic Sea Research

Seestr. 15

18119 Rostock

Submitted to "Progress in Oceanography"

31.7. 2024

Revised version 1: 25.6.2025

Revised version 2: 12.8.2025

Highlights

● Climate regime shifts do not necessarily cause biological regime shifts.

● Linear forcing with multiple drivers can cause abrupt biological regime shifts.

● Riverine nutrient inputs is modulated by sewage treatment plants and variable precipitation.

● Stable isotope values of two macrofaunal species indicated specific feeding modes.

● Regime shifts and de-eutrophication change macrofaunal feeding behavior and biomass.

● A biological memory of 3 years was due to an internal North Atlantic climate mode.

Abstract

This study analyzed the potential influence of multiple drivers, such as climate variability and regime shifts, on benthic life using long-term data sets describing the abundance, biomass, and stable isotopes (1978–2017) of two benthic species in the southern North Sea, generated from preserved samples. Specifically, changes in nitrogen supply and trophic position were identified by bulk and amino-acid-specific isotope analyses of the native warm–temperate bivalve *Fabulina fabula* and the native cold–temperate polychaete *Magelona* spp., which together made up > 60% of the biomass and abundance of all benthic animals in the original samples. Bulk stable isotopes ratios of total carbon and nitrogen as well as amino-acid specific-isotope ratios were corrected with respect to the preservation method. Statistical downscaling and a scanning *t*-test were applied to various time series of climate, Rhine and Maas riverine runoff, and local monitoring at the island of Norderney. The scanning *t*-test identified three regime shifts in the drivers and macrofaunal responses, which allowed four regimes, occurring during the periods 1978–1988, 1989–2000, 2001–2009, and 2010–2017, to be distinguished.

Quantitative metrics using a phenotype-based approach were computed for all data and for the four identified regimes, to characterize aspects of the trophic position and functional diversity of the two macrofaunal species. Functional diversity in a single species decreased over time, indicating a normalization of feeding habits and increased productivity under decreasing nutrient loads, a shift in biomass from specialist to generalist, and an increase in stability and resilience after 2000. Based on the de-correlation time, an ecological memory of the system of ~3 years was identified for *F. fabula* and *Magelona* spp., attributable to an internal basin mode in climate variability driven by atmosphere–ocean interactions in the North Atlantic.

Keywords: Climate regime shift, de-eutrophication, macrofauna, stable isotopes, trophic level, functional diversity, ecological memory, southern North Sea

1. Introduction

Climate change, nitrogen footprints, and biodiversity loss are among the global indicators that have already passed beyond the well-defined thresholds of Earth's boundaries and may eventually result in disastrous consequences (Rockström, 2009; Zhang et al., 2015; Glibert & Burfort, 2017). Marine coastal ecosystems around the world are currently undergoing dramatic changes because of human activities such as climate change, fisheries activity or tourism, such that species diversity has significantly declined (Worm et al., 2006; Steffen et al., 2007). Benthic communities are dominated by only a few species in the North Atlantic (Birchenough et al., 2015) and until the 1990s, pelagic–benthic coupling processes and food supply are the main factors determining the variability of the benthos in the North Sea, followed by many other factors, none of which was dominant on its own (Frid et al., 2009). While factors such as eutrophication and water temperature can act as drivers of changing species composition, their effects may be masked by a complex network of anthropogenic drivers, such as habitat loss, more intense storms, and acidification.

Changes in ecosystem stability can best be investigated during disturbances that occur in association with transient events such as regime shifts (RSs). The theoretical framework of RSs is well developed with respect to RSs involving top-down trophic cascades (Pershing et al., 2015; Rocha et al., 2018) and bottom-up physical drivers such as climate regime shifts (CRSs) (Smith, 2011; Conversi et al., 2015; Beaugrand & Kirby, 2018; Hastings et al., 2018). The term "biological regime shift" (BRS) refers to a large, sudden, and long-lasting change in the dynamics of an ecosystem that affects all trophic levels and multiple physical components (Aebischer et al., 1990; Reid et al., 1998; Spencer et al., 2011, Dippner et al., 2019). Several BRSs occurred during the last century, at different locations across the world (e.g., Mantua et al., 1997; Peterson and Schwing, 2003; Beaugrand et al., 2015; Reid et al., 2016).

Although there is no consistent definition of a BRS (deYoung et al., 2004), Scheffer et al. (2001) classified them into three different types (smooth, discontinuous, and abrupt) linked to the linearity or non-linearity of the driving external processes, such as climate change, CRSs, and biological interactions. In this classification, a smooth BRS is described by a quasi-linear relationship between the driver and the response variables (de Young et al., 2004), while in a discontinuous BRS, alternative stable states might occur (Collie et al., 2004), and an abrupt BRS is represented by a non–linear relationship between the driver and the response variables. An understanding of extreme climate events can lead to the development of a mechanistic understanding of how they affect biological processes, ecosystem functioning (Ummenhofer & Meehl, 2017; Turner et al., 2020).

In the North Sea and the Baltic Sea, the North Atlantic Oscillation (NAO, Hurrell, 1995) strongly influences the abundance, biomass, and species number of macrozoobenthos (Kröncke et al., 1998; 2013; 2019 and references therein; Dippner & Ikauniece, 2001). Recent analyses in the southern North Sea indicated that, besides climate variability, de-eutrophication and epibenthic abundance contribute to inter-annual biological variability (Meyer et al., 2018; 2019; Meyer & Kröncke, 2019; van Beusekom et al., 2019). The impact of CRS is also reflected in feeding modes, distribution types, and taxonomic groups (Dippner et al., 2014), but not in food web dynamics or in functional diversity (FD).

Food web dynamics and FD can be obtained by analyzing stable isotope ratios of carbon ($\delta^{13}C$) and nitrogen ($\delta^{15}N$) to quantify, for example, nutrient flows, the structure of food webs (Vander Zanden et al. 1999; Fry, 2006) and trophic position (DeNiro & Epstein, 1978; 1981; Minagawa & Wada, 1984; Post, 2002). In combination with the results of modeling approaches (Cornwell et al., 2006; Layman et al., 2007), stable isotope data provide information on trophic diversity within a food web, trophic redundancy, niche diversification, and the distribution of trophic niches.

Bulk nitrogen isotope ratios contain information on the changes in the N source and trophic position (TP) of an organism. To disentangle these factors, compound-specific nitrogen stable-isotope analyses (CSIAs) of amino acids (AAs) can be applied. The strength of CSIA lies in providing information on both TP and N sources from a single biological sample, which is achieved with a comparison of the $\delta^{15}N$ values of two different groups of amino acids (AA), the source AAs and the trophic AAs. While trophic AAs including alanine, valine, leucine, isoleucine, proline, and glutamic acid are enriched in ^{15}N by ~8.0‰ per trophic transfer (Chikaraishi et al., 2009), the $\delta^{15}N$ of source AAs including phenylalanine, glycine, serine, tyrosine, lysine, methionine and histidine remain nearly unchanged when the AA is transferred through the food web and thus they reflect the isotopic composition of the primary producers (N source measure; McClelland & Montoya, 2002; Chikaraishi et al., 2010; O´Connell, 2017). Among all AAs, the trophic AA Glutamic acid (Glu) and the source AA Phenylalanine (Phe) is the most robust and frequently used pair to estimate the TP in marine invertebrates (McClelland & Montoya, 2002; Chikaraishi et al., 2010). With the $\delta^{15}N$ ratio of both amino acids and the trophic discrimination factor (TDF) that is specific for different groups of organisms, the TP of invertebrates like macrozoobenthos can now be calculated empirically with an accuracy of 0.1–0.2 units.

Time series of stable isotopes are hardly used in marine ecology studies. To our knowledge, only Wainright et al. (1993) analyzed total carbon and nitrogen isotopes in their study of the long-term changes in the trophic structure of seven species of demersal fish from the Georges Bank food web. The authors found a significant correlation between haddock and the Greenland regional pressure anomaly and the NAO.

Based on these studies, we analyze benthic organisms of the Wadden Sea over a period of 40 years, potentially reflecting changes in nutrient and food sources. Our study examined the impact of multiple potential drivers on various trophic aspects and on the FD of two representative species of benthic macrofauna in the southern North Sea: *Magelona* spp. and *Fabulina fabula*. During a sampling period from 1978 to 2017, these two species dominated the benthos and can thus be used as indicators of the environmental changes that occurred during that time. The focus of our study was the following: (1) the environmental impacts on *Magelona* spp. and *F. fabula* during the time series and the responses of these species in terms of nutrition, trophic position, and FD; (2) a demonstration of how the application of a hierarchy of chosen methods can provide a deeper understanding of benthic ecosystems. The lab methods and complex hierarchy of the mathematical analyses are described in Chapter 2 “Material and Method” and summarized in Figure 1, which also shows the links between the individual steps of the analysis in a holistic view. We demonstrate that the knowledge of abundance and biomass of macrozoobenthos species and their stable

isotopes and the application of different models provide information on trophic position, trophic specialization niche differentiation, redundancy, competition, productivity, buffer capacity and ecological memory.

2. Material and Methods

2.1 Study area and selected species

Quarterly sampling was carried out from 1978 to 2017 at five different stations in the sub-littoral zone off the island of Norderney (southern North Sea) at a water depth of 10–20 m (Fig. 2). The sampling stations were located in an area without thermal stratification due to strong tidal mixing, which cause higher pelagic–benthic coupling. The long-term study of benthic macrofauna is part of Senckenberg´s Long-Term Ecological Research (LTER) in the North Sea (Kröncke et al., 2019). The study area was considered representative of the entire coastal area of the southeastern North Sea because the *F. fabula* population occurs on fine sands like those in the study area (Kröncke, 2011; Kröncke et al., 2013). In this area, *Magelona* spp. is a dominant species within the *F. fabula* community. In contrast to 1980s taxonomy, Fiege & Mackie (2000) identified *Magelona johnstoni* to be the dominant Magelonid species in the study area.

Samples from all stations were treated as replicates for the area, since a multivariate comparison showed no significant differences between their macrofaunal communities (Dörjes et al., 1986). Abundance and biomass of the two dominant benthic macrofaunal species were selected for this investigation: the native warm–temperate bivalve *F. fabula* (interface or suspension feeder) and the native cold–temperate polychaete *Magelona* spp. (detritus feeder and predator) (Jones, 1968; Uebelacker & Jones, 1984; Fiege et al. 2000; Mortimer & Mackie, 2014; Jumars et al. 2015). Although more than 190 taxa were identified in the study region (Kröncke et al., 2013), the two selected species accounted for up to > 60% of the total abundance and biomass and provide enough material for isotopic analyses. Samples obtained during the 2nd quarter of each years were used in the isotope analyses because earlier statistical analyses showed significant correlations of 2nd quarter species number, abundance, and biomass with climate variability (Kröncke et al., 1998; 2013; Dippner & Kröncke, 2015).

2.2 Sampling, sample preservation, and sample preparation

Macrofaunal abundance and biomass were determined in samples collected using a 0.2-m^2 van Veen grab. The samples were sieved over a 0.63-mm mesh size and fixed in 4% buffered formalin solution. After their taxonomic identification, the organisms were preserved in 70% ethanol. The ash-free dry weight of the samples was determined after drying the samples for 24 h at 85°C and then burning them for 6 h at 485°C.

For the isotope analyses, the *F. fabula* and *Magelona* spp. specimens from 1978–1996 were taken from sorted replicate samples preserved in 70% ethanol, while specimens from 1997–2017 were taken from unsorted formalin-fixed replicate samples. The latter were rinsed prior to further treatment, whereas the ethanol-fixed samples were removed from the vials and the excess ethanol was allowed to drip off the sample. All samples were weighed (wet weight) to ensure that enough material was available for the isotope analysis. The shells of *F. fabula* were removed before the bivalve was weighed because the isotopic signal in shells reflects carbon chemistry of water

instead of food sources (Fry 2006). After drying overnight at 50°C in a drying oven, the samples were weighed again (dry weight) and transferred to small glass vials. At least 35 mg (wet weight) of each species (usually several individuals) was needed to obtain the 3–4 mg of dry material allowing the analysis of triplicates. Only single values are reported for 2016, because the amount of material did not suffice for triplicate samples. The samples were homogenized with a mortar and pestle, after which 0.8–1 mg of the homogenized material was packed into tin caps and analyzed on an isotope ratio mass spectrometer (IRMS).

2.3 Stable isotope analysis and preservative correction

Stable isotopes of carbon and nitrogen ($\delta^{13}C$, $\delta^{15}N$) were measured using a Thermo Scientific Delta V Advantage IRMS combined with a Conflo IV interface and a Flash 2000 elemental analyzer. Reference gases were calibrated using IAEA standards N1, N2, and N3. The precision of the measurements was ≤ ±0.2‰ for the carbon and nitrogen isotope data. Values were calculated using standard δ notation and expressed as a ‰ using Eq. (1) (Peterson & Fry, 1987):

$$\delta X = \left[\frac{R_{\text{sample}}}{R_{\text{standard}}} - 1 \right] * 1000 \quad (1)$$

where δX is $\delta^{13}C$ or $\delta^{15}N$ and R is the corresponding ratio, ^{13}C:^{12}C or ^{15}N:^{14}N, respectively. A prerequisite of a meta-analysis of stable isotopes is the correction of the isotopic values of the preserved samples with respect to the preservation method, here, either ethanol or formalin. The impact of formalin (CH_2O) and ethanol (C_2H_6O) preservation on the isotopic composition was corrected according to Umbricht et al. (2018), by applying the correction factors to the measured $\delta^{13}C$ and $\delta^{15}N$ time series of *F. fabula* and *Magelona* spp. (Figs. 3, 4) and to the measured $\delta^{15}N$ of the N-source AA Phe.

2.4 Compound-specific isotope analyses of amino acid nitrogen (CSIA)

Amino acid $\delta^{15}N$ values were determined on a subset of 25 samples for both specimens. All samples used in the CSIA analysis were from the 2nd quarter, with the exception of *F. fabula* from November and December 1990, included due to biomass limitations. For the CSIA, ~20 mg of each dried and powdered *F. fabula* or *Magelona* spp. tissue sample was transferred into a heat-resistant borosilicate vial, mixed with 5 ml of 6M HCl and 1 ml of internal standard (trans-4 (amino methyl)-cyclohexane carboxylic acid), and hydrolyzed for 24 h at 110°C. The samples were then filtered through cellulose-acetate filters, dried under a nitrogen flow at 50°C, and derivatized to TFA-isopropyl amino esters (Silfer et al., 1991; Hofmann et al., 2003), which included an additional purification step using a chloroform-phosphate buffer solution (Veuger et al., 2005). The derivatized samples were dissolved in 500 µl of methylene chloride and stored in GC-vials at −20°C until analyzed as described below.

The TFA-isopropyl-derivatized samples were analyzed for the $\delta^{15}N$ content of 13 AAs: alanine (Ala), glycine (Gly), threonine (Thr), serine (Ser), valine (Val), leucine

(Leu), isoleucine (Ile), proline (Pro), aspartic acid (Asp), glutamic acid (Glu), phenylalanine (Phe), tyrosine (Tyr), and lysine (Lys). An external standard containing 16 AAs was also included. Isotope value accuracy was checked by comparison of the internal trans-4 (amino methyl)-cyclohexane carboxylic acid standard with its known value, and by assessing values of an in-house amino acid mix as external standard, analyzed with every sample set. Reproducibility, as estimated with standard deviation for samples, was on average less < 0.5‰ (range: 0.1–0.8‰) for both Glu and Phe. The concentrations of cysteine, arginine, and methionine in the samples were below the qualitative limit of detection of the measurement device and could therefore not be determined. During the initial hydrolysis step, glutamine (Gln) and asparagine (Asn) were converted into glutamic acid and aspartic acid, respectively, and are reported as Glu + Gln (referred to herein as Glu) and Asp + Asn (Asp).

AA-specific $\delta^{15}N$ values were measured using an IRMS (Thermo Finnigan GmbH, 253 Plus MS, Germany) connected via a ConFlo IV interface unit to a gas chromatograph and combustion oven (GC-C); Helium was the carrier gas (Thermo Scientific Trace 1310 GC, Italy; Thermo Scientific, GC Isolink, Germany). The separation column in the GC consisted of a non-polar column coated with 5% phenyl-polysilphenylenesiloxane (BPX5, 60 m, 0.32 mm inner diameter, film thickness of 1 µm; SEG Analytical Science, Ringwood, Victoria, Australia). For each run, 2 µl of sample was injected via a PTV injector in splitless mode. The temperature program was as follows: initial temperature 60°C, hold for 1 min, heat at 14°C/s to 250°C, and hold for 6 min. Each sample was injected and measured at least three times. The standard deviation from three runs was usually <1.0‰ for all 13 AAs. The obtained AA-specific $\delta^{15}N$ values were also corrected using the correction factors of Umbricht et al. (2018).

2.5 Additional data

In addition to the time series of both species, our study included monthly climate, river, nutrient, and benthic time series. As climate data, the NAO index (Hurrell, 1995), the North Sea Environmental (NSE) index (Dippner & Kröncke, 2015), the sea surface temperature (SST) in the southern North Sea, and the precipitation rates over the catchment of major central European rivers (Kalnay et al., 1996) were used (Fig. S1). NAO is the dominant mode of atmospheric variability in the Atlantic sector and has been widely applied to identify the response of climate variability in marine ecosystems (Drinkwater et al., 2003 and references therein; Dippner, 2006). The NSE index is a multivariate climate index consisting of five different global and regional time series; it has a better potential predictability than the NAO, especially after the CRS that occurred around 2000 (Dippner et al., 2014; 2015). Re-analysis data of the National Center of Environmental Prediction/National Center of Atmospheric Research (NCEP/NCAR) (Kalnay et al., 1996) were used to extract monthly SST data in the southern North Sea for the area 53°–54°N and 7°–8°E, and monthly precipitation rates over the catchment area 46°–56°N and 5°W–15°E (Fig. S1).

The potential impact of de-eutrophication and a decreasing food supply (Meyer et al., 2018; 2019; van Beusekom et al., 2019) were investigated using the monthly mean data of the total discharge, cumulative total discharge, and total nitrogen and total phosphorus loads from the Rhine and Maas rivers for the period 1977–2017 (Fig. S2)

and monthly monitoring data of SST, sea surface salinity (SSS), NH_4^+, NO_2^-, NO_3^-, PO_4^{3-}, SiO_4, chlorophyll-*a* (Chl-*a*), and suspended particulate matter (SPM) recorded at Norderney for the period 1985–2016 (Figs. S3, S4; van Beusekom et al., 2019). Riverine nutrient input data were initially compiled by Lenhard and Pätsch (2004) and updated to 2017 (van Beusekom et al., 2019) and detrended (Fig. S2).

Our study also included time series of the abundance, biomass, stable isotopes and species number of the total macrofauna in the southern North Sea (Figs. S5–S7). All monthly time series were standardized (zero mean and unit standard deviation) and filtered for the plots by applying a low-pass filter with a cutoff period of 25 months, using the filter weights of Schönwiese (2000). To investigate the potential impact of different spatial precipitation patterns in central Europe, precipitation rate anomalies were plotted as composites for different regimes using NCEP/NCAR re-analysis data (Fig. 5, Kalnay et al., 1996).

2.6 Statistical downscaling

A statistical downscaling method (von Storch et al., 1993) was used to detect relationships between global climate predictors and regional predictands. First, empirical orthogonal functions (EOF) of the anomalies of global climate predictors $\breve{G}'(\breve{x},t)$ and of local predictands $\breve{L}'(\breve{x},t)$, both of which are functions of space $\breve{x}$ and time *t*, were calculated, as shown in Eq. (2):

$$\breve{G}'(\breve{x},t) = \sum_{i=1}^{K} \breve{\Gamma}_i(\breve{x})\gamma_i(t) + noise$$
$$\breve{L}'(\breve{x},t) = \sum_{i=1}^{K} \breve{\Lambda}_i(\breve{x})\lambda_i(t) + noise \quad (2)$$

The major part of the variance from a multidimensional vector is therefore concentrated in a few new dimensions, the leading *K* eigenmodes. The advantages of this approach are that the dimensionality of the model is kept low and noise is reduced. Second, a canonical correlation analysis (CCA) was performed between the leading eigenmodes such that the time series correlated optimally with each other. Hence, following Heyen and Dippner (1998), the regional time series was regressed from the climate predictor using Eq. (3):

$$\breve{L}'(\breve{x},t) = \sum_{i} \breve{\Lambda}_i(\breve{x})\rho_i\gamma_i(t) \quad (3)$$

where ρ is the correlation coefficient of the CCA coefficients. From the tested combinations, the results with the highest skills were selected. As skill factors, the correlation coefficient r (between the regional observations and the cross-validated estimations) and, as a measure of the explained variance, the Brier-based score β were used. The Brier-based score is defined as: $\beta = 1 - \sigma_E^2 / \sigma_O^2$, where σ_E^2 and σ_O^2 are the variances of the error (i.e., observation minus model) and observations. $\beta=1$ means that the model and the observation are identical, and $\beta=0$ that the error of the model has the same size as the variance of the observations (Livezey, 1995). The model was validated using cross-validation (Michaelsen, 1987) and Monte Carlo (Livezey, 1995) techniques. A detailed description is provided in Dippner et al. (2001). Statistical

downscaling was applied to the time series using the climate, river, and local monitoring data as predictors and the benthic time series as predictands. The identified downscaling relations are shown in Figs. 6a-6e and Table 1.

Different predictor fields for climate variability, river runoff, regional monitoring, and predictand fields were constructed for *Magelona* spp. and *F. fabula*. The NSE index served as a multivariate climate predictor (Dippner et al., 2015), and the four dominant EOFs, with an **e**xplained **v**ariance (ev) of 92% were used. The river runoff predictor consists of four different monthly mean time series: total discharge, cumulative total discharge, total nitrogen loads, and total phosphorus loads (Van Beusekom et al., 2019). For this predictor, the two dominant EOFs (ev 94%) were used. The regional monitoring predictor consists of nine monthly time series obtained at Norderney: SST, SSS, NH_4^+, NO_2^-, NO_3^-, PO_4^{3-}, SiO_4, Chl-*a*, and SPM. Here, the six dominant EOFs (ev 80%) were used.

The biological predictand field of *Magelona* spp. was constructed using four time series: annual $\delta^{15}N$, $\delta^{13}C$, abundance, and biomass. The three dominant EOFs (ev 95%) were used. The same procedure and the three dominant EOFs (ev 93%) were applied to *F. fabula*.

Single climate and river runoff time series were also examined, including the NAO index, the precipitation rate over the catchment areas of major European rivers (Fig. 5), and the SST of the German Bight, and related to stable isotope time series to identify further potential drivers. In this case, Eq. (3) was reduced to a plain regression. Significant combinations identified in this analysis are shown in Table 1.

2.7 Scanning *t*-test

Climatologic time series are often serially correlated. In those cases, a classical *t*-test is not applicable (Zwiers & von Storch, 1995). Thus, in this study a scanning *t*-test was applied to all time series to identify multi-scale abrupt BRSs, which should occur simultaneously with potential CRSs (Schwing et al., 2003). The scanning *t*-test identifies statistically significant changes in a time series based on calculations of the contrasts between subsets of the data (Jiang et al., 2002). A statistic *t(n,j)* of the scanning *t*-test for a subsample size *n* at point *j* is defined as shown in Eq. (4):

$$t(n,j) = (\bar{x}_{j2} - \bar{x}_{j1}) * n^{1/2} * (s_{j2}^2 + s_{j1}^2)^{-1/2} \quad (4)$$

where [Eq. (5)]:

$$\begin{aligned}
\bar{x}_{j1} &= \frac{1}{n}\sum_{i=j-n}^{j-1} x(i) \\
\bar{x}_{j2} &= \frac{1}{n}\sum_{i=j}^{j+n-1} x(i) \\
s_{j1}^2 &= \frac{1}{n-1}\sum_{i=j-n}^{j-1} (x(i)-\bar{x}_{j1})^2 \\
s_{j2}^2 &= \frac{1}{n-1}\sum_{i=j}^{j+n-1} (x(i)-\bar{x}_{j2})^2
\end{aligned} \tag{5}$$

The subsample size $n = 2, 3, \ldots, <N/2$ is the length of the period being compared; the tested reference point is $j = n+1, n+2, \ldots, N$ (Schwing et al., 2003). The "table-look-up test" (Zwiers & von Storch, 1995, Table 7) was used as a correction for the autocorrelation in the time series. For every sub-sample, the critical *t*-value was computed based on the pooled sample lag–1 autocorrelation coefficient and the sub-sample size using Eq. (6):

$$t_r(n, j) = t(n, j) / t_\varepsilon \tag{6}$$

Multi-scale abrupt changes occurring in all sub-samples at the same time can be interpreted as the occurrence of a RS, which is significant at a confidence level $\varepsilon=0.05$ when $|t_r(n,j)|>1$. The sign of $t_r(n,j)$ indicates an abrupt increase or decrease. The scanning *t*-test is an alternative to other methods in the identification of RSs (Rodionov, 2004; Spencer et al., 2011) and in this study it was applied to nearly all time series (Fig. 7 and Figs. S8–S13). Unfortunately, a gap in the time series of stable isotopes prevented the application of a scanning *t*-test.

2.8 The Layman model

The Layman model (Layman et al., 2007), a phenotype-based approach for analyzing community structure (Cornwell et al., 2006; Pausas & Verdu, 2010; Karlson et al., 2015) provides information on trophic diversity, trophic redundancy, niche diversification, and the distribution of trophic niches. In this study it was applied to the corrected isotopic values to analyze both the differences between the dominant species and the changes in their trophic structure over a period of 40 years. Although considered a community-wide measure of trophic structure, the Layman model is also applicable to single species (Winemiller, 1990). It consists of six community-wide metrics that reflect important aspects of trophic structure: 1) the range of $\delta^{15}N$ data (*NR*) is a measure of the diversity of trophic levels and represents the vertical food web structure, also called vertical biodiversity (Duffy et al., 2007); (2) the range of $\delta^{13}C$ data (*CR*) is a measure of the diversity of consumed food sources (Gonzalez-Bergonzoni et al., 2015) and represents niche diversification at the base of the food web; 3) the convex hull area (*TA*) is a measure of the total trophic diversity in a food web and the smallest convex polygon containing all species in the $\delta^{13}C$–$\delta^{15}N$ bi-plot space (Fig. 8); 4) the mean Euclidean distance to the centroid (*CD*) is computed as the mean $\delta^{13}C$ and $\delta^{15}N$ values for all species in the food web and is considered as a measure of the averaged degree of trophic diversity; 5) the mean nearest Euclidean

neighbor distance (*NND*) is a measure of the overall density of species packing and trophic redundancy; and 6) the standard deviation of the mean nearest neighbor distance (*SDNND*) is a measure of the evenness of species packing and trophic redundancy.

The construction of *TA* was as follows: The minimum $\delta^{13}C$ value, which, by definition (De Berg et al., 2008), is part of the convex hull, served as the starting point from which the slope to every other data point was computed and then sorted in ascending order, excluding the starting point, using the sorting algorithm iindexx (Press et al., 1992). The end points of the sorted slopes form a polygon. The 'three penny algorithm' (Graham, 1972) was then used to compute the vertices from the polygon, which define the convex hull. Details are given in Umbricht et al. (2018).

This method has generated criticism especially when the convex hull is used as a measure of trophic niche width. Among the issues that have been raised is the sensitivity of the metrics with respect to the number of individuals, as the convex hull and the distance to the centroid are very sensitive (Brind'Amour & Dubois, 2013; Syväranta et al., 2013). The same sensitivity occurs in these metrics if stable isotope ellipses are used (Jackson et al., 2011). However, Rigolet et al. (2015) found that problems with the convex hull computation can be resolved by the use of different methods described by Layman & Post (2008) and Brind'Amour et al. (2009). These arguments reason of our decision to apply a complex model hierarchy to the stable isotope data sets of the benthic species.

2.9 Nitrogen source and trophic position estimations

The $\delta^{15}N_{Phe}$ value was used as an indicator of the inorganic nitrogen source for *F. fabula* and *Magelona* spp. (Loick-Wilde et al., 2019), and the $\delta^{15}N_{Glu}$ value as an indicator of the AA integrating trophic effects. TP was then computed from the difference between $\delta^{15}N_{Glu}$ and $\delta^{15}N_{Phe}$ with respect to the trophic discrimination factor (TDF), after Choi et al. (2018), as shown in Eq. (7):

$$TP = \frac{(\delta^{15}N_{Glu} - \delta^{15}N_{Phe} - \theta)}{TDF} + 1 \qquad (7)$$

where θ is the isotopic difference between $\delta^{15}N_{Glu}$ and $\delta^{15}N_{Phe}$ in cyanobacteria and algae and is equal to 3.4‰ (Chikaraishi et al., 2009). Because the TDF value is lower for benthic organisms than for pelagic invertebrates, due to the mucus synthesis used for settlement ability or feeding by the former, it needs to be adjusted to obtain a correct TP estimation (Choi et al., 2018). Mean TPs of 2.0 and 2.5 were expected for *F. fabula* and *Magelona* spp., respectively (Jumars et al., 2015). Three values (3.0, 5.3, and 7.5) of TDF, consistent with the turnover by those gastropods (and possibly other benthic organisms) of different amounts of proteinaceous mucus, were tested (Choi et al., 2018). Only the lowest value created TP values in the range expected from observations; the other two TDF values resulted in TPs that were too low for deposit and suspension feeders (Maeda et al., 2012; Amorim et al. 2022)

Multivariate correlations of the CSIA data were used to identify the biotic and abiotic factors from the nine regional monitoring data sets that affected the mean N-source

and TP of the two macrozoobenthos species. Both benthic data and environmental variables were time-integrated to identify maximum correlations (Figs. S15, S16).

2.10 Functional diversity

Functional diversity can be split into three components: isotopic functional richness (IFR), isotopic functional evenness (IFE), and isotopic functional divergence (IFD). IFR is a measure of the amount of functional space occupied by a community in an *n*-dimensional trait space. A low IFR indicates a reduced productivity (Petchey, 2003) or a decreased buffer capacity against environmental fluctuations, such as food sources (Mason et al., 2005). IFE provides information on the distribution of the biomass of a community in the isotopic functional space. A low value indicates that the community is composed of clusters of species and implies trophic redundancy and food competition; a high value indicates an even distribution that could result in greater productivity, stability, and resilience (Hooper et al., 2005). IFD provides information on the filling of the isotopic functional space. A high value indicates that biomass-dominant species occupy the isotopic space more densely at its edges; these species are likely to exhibit trophic specialization and a high degree of niche differentiation (Rigolet et al., 2015). A low values indicate that the species are closer to the center of gravity, implying that their total biomasses is dominated by generalists.

Three different measures are used to calculate FD (Petchey et al., 2009): measures based directly on traits (Cornwell et al., 2006), measures based on a distance matrix (Walker et al., 1999), and measures that include a functional dendrogram (Petchey & Gaston, 2002; Podani & Schmera, 2006). However, there is no consensus on which is the most suitable (Petchey et al., 2009; Flynn et al., 2011) or which traits are the most relevant. If stable isotopes are used as traits, then FD can be calculated from the output of the Layman model: the minimum total area *TA* serves as a proxy for IFR, the mean nearest neighbor distance *NND* for IFE, and the mean Euclidean distance to the centroid *CD* for IFD.

Hoeinghaus and Zeug (2008) concluded that isotope bi-plots are not appropriately scaled for these measures, and Cornwell et al. (2006) that the data should be standardized before computing volumes. Therefore, in this study the calculations of IFR, IFE, and IFD were repeated using a standardized data set of stable isotopes.

2.11 Memory of the system

According to von Storch and Zwiers (1999), the autocorrelation function *α(k)* described by Eq. (8):

$$\alpha(k) = \frac{Cov(X_t, X_{t+k})}{Var(X)} \tag{8}$$

can be used to compute the de-correlation time defined as shown in Eq. (9):

$$\tau_D = \left[1 + 2\sum_{k=1}^{\infty} \alpha(k)\right]\Delta t \quad (9)$$

where Δt is a time increment, and the dimensionless de-correlation time (the term in square brackets) is a statistical quantity included as a characteristic time scale when dealing with serially correlation observations, such as red noise processes or long-term climate variability. Multiplying the de-correlation time by a time increment Δt results in a characteristic time scale, which is in the red noise case with $\alpha(1)>0$ equivalent to the memory of the system (von Storch & Zwiers, 1999). The ecological memory, i.e., the role of time in ecology, is important for understanding species responses to rapid disturbances and RSs; it also defines the time scale over which an ecological process is shaped by its past modification (Peterson, 2002).

Identification of the climate and ecological memory of a system using the de-correlation time is an alternative to methods based on autocorrelation functions (Peterson, 2002; Ogle et al., 2015) and can be applied to all time series. The lag $\alpha(1)$, the memory (de-correlation time) of the system, and the same sample size used in the scanning *t*-test are displayed in Table 2.

3. Results

3.1 Abundance and biomass

The time series of the abundance and biomass of *Magelona* spp. and *F. fabula* (Fig. 3) indicated that both species had a pronounced inter-annual variability and made up a relatively large share of the total benthic biomass: 0–33% for *Magelona* spp. and 2–61% for *F. fabula.* In the time series of *Magelona* spp., the species accounted for up to 30% of total biomass during the cold period between 1978 and 1988. After the major CRS in 1988/89 (Reid et al., 2016), marked by a warming period, the abundance and biomass share of *Magelona* spp. decreased strongly, except in 1995, when a very cold winter occurred (Dippner et al., 2014). The abundance and biomass of *F. fabula* was highly variable over the 40-year period, with major peaks in 1985, 1999, 2001, 2010, and 2013. During the cold period, the amplitudes were in the same range as those of *Magelona* spp., except in 1985. After 2000, the abundance of the warm water species *F. fabula* increased. The highest percentage of biomass (> 50%) for *F. fabula* occurred after 1997. For the two species, the strongest peaks, i.e., those indicating > 40% of total biomass, occurred in 1985 (65.5%), 1989 (53%), 1995 (45%), 1999 (67%), 2000 (55%), 2001 (62%), 2010 (63.5%), and 2013 (43%). Of these, the peak during the extreme winter in 1995 was attributable solely to *Magelona* spp.; all other peaks were dominated by *F. fabula* with the exception of the peak in 1989. The year of the transition from a cold to a warm period influenced both species: the abundance of the cold water species *Magelona* spp. decreased, whereas the abundance of *F. fabula* increased.

3.2 Correction of isotope values due to the preservation method

Preservation methods—whether freezing, drying, freeze–drying, conservation in salt, fixation or preservation in Lugol's solution, formalin, ethanol, formalin–ethanol, or lipid-extracted formalin or lipid-extracted ethanol (Umbricht et al., 2018 and references therein)—change the stable isotope ratios in animal tissues in different ways (Bosley & Weinright, 1999). In our study, the stable isotope values were corrected for the respective preservation medium according to Umbricht et al. (2018). The corrections had a stronger impact (up to 3‰) on carbon isotopes than on nitrogen isotopes (Fig. 4), in good agreement with observations in the literature.

The corrected ^{15}N values of *F. fabula* decreased significantly after 1990, while the corrected ^{13}C values increased after 1990. The corrected ^{15}N values in *Magelona* spp. were rather similar over time, while the corrected ^{13}C values were lowest in 1990 and 2000 but increased thereafter.

3.3 Precipitation and river runoff

The cumulative discharge data of the Rhine and Maas rivers (Fig. S2) showed two major CRSs, represented by a change in the trends in 1988/89 and in 2003/04, that could be linked to the inter-annual variability in precipitation. The composites of precipitation during the three regimes 1978–1988, 1989–2003 and 2004–2017 are

displayed in Fig. 5. The anomalies of the precipitation rate were positive in central Europe in 1978–1988, indicating stronger than normal precipitation in the catchments of major European rivers during the cold period (Fig. S1). The period 1989–2003, which includes the warm period 1989–2000 (Fig. S1), was characterized by a dry period with negative anomalies in the precipitation rate in central Europe. After 2004, those anomalies had a heterogeneous pattern, with local centers of strong precipitation over the Irish Sea, southern Norway, and the Alps. These different and variable patterns drove the inter-annual variability in river discharge. However, beginning in 1981, decreasing trends in the time series of total nitrogen and total phosphorus were detected, as several sewage treatment plants became operative (van Beusekom et al., 2019).

3.4 Statistical downscaling

The first and second CCA patterns for the predictors (black) and predictands (red) were plotted in a vector space (Fig. 6). To avoid confusion, the reader should note that this graph is not a canonical correspondence analysis. The fitting coefficients of the predictors (black) and predictands (red) were plotted as a time series and showed the strong correlations. The identified downscaling relations for all computations are shown in Table 1.

When the NSE index was used as the climate predictor, no meaningful result was obtained for the *Magelona* spp. predictand. By contrast, *F. fabula* showed a significant correlation and a significant skill, with a time lag of 2 months for the five variables comprising the NSE index (Fig. 6a). In this computation, the explained variance of the second CCA pattern of the predictor was larger than that of the first. This may have occurred because the time coefficients of the CCA are a weighted linear combination of the EOF coefficients under the constraint of an optimal correlation. The eigenvectors of the dominant CCA patterns indicated a positive correlation between AO, zonal wind, and $\delta^{15}N$, and a negative correlation between $\delta^{13}C$, abundance, and biomass. Weakly negative correlations were determined between $\delta^{15}N$ and both precipitation and SST, and positive correlations between $\delta^{13}C$ and abundance and biomass.

Applying the riverine variables as a predictor resulted in different significant correlations, all with a lag of 9 months. For *Magelona* spp., strongly positive correlations of abundance and biomass with river discharge as well as nitrogen and phosphorus loads were determined (Figs. 6b). $\delta^{15}N$ correlated negatively with these three variables in the predictor field whereas $\delta^{13}C$ showed a spurious correlation. No correlations with cumulative river discharge were identified.

In the downscaling experiment of the river predictor for the *F. fabula* predictand, an opposite signal was obtained, consisting of a positive correlation of $\delta^{15}N$ and a negative correlation of both $\delta^{13}C$ and abundance with river discharge and nitrogen and phosphorus loads (Figs. 6c). No major role was played by cumulative river discharge or the biomass of *F. fabula*. The behaviors of the trends and inter-annual variability in the time coefficients were similar to those of *Magelona* spp., especially the decrease in the amplitudes after 1995. An experiment using a de-trended time series for total

nitrogen and phosphorus produced similar results, but with smaller correlation coefficients (not shown).

Applying the regional monitoring data as the predictor resulted in heterogeneous patterns and correlations without any time lag. With *Magelona* spp. as predictand, SSS and NO_3^- correlated positively with $\delta^{13}C$, abundance, and biomass, and negatively with $\delta^{15}N$ (Fig. 6d). With *F. fabula* as predictand, $\delta^{13}C$, abundance, and biomass correlated positively with SSS and SPM, and negatively with SST, NO_2^-, NO_3^-, and PO_4^-. Opposite results were obtained for $\delta^{15}N$ (Figs. 6e). None of these downscaling combinations resulted in a correlation with Chl-*a*.

The time coefficients of the predictors and predictands in all of the downscaling experiments were highly correlated, and the trends and amplitudes of the inter-annual variability, especially for the extremely cold winter of 1995/96, were well reproduced.

No significant results for stable isotopes were obtained when the NAO or the precipitation rate was used as the predictor. With the NSE index, the four dominant EOFs, and the SST, $\delta^{13}C$ and $\delta^{15}N$ signals were obtained for *F. fabula* but not for *Magelona* spp.. Only river runoff showed a response in the $\delta^{15}N$ values of both species: for discharge and total load in *Magelona* spp. and for total nitrogen and total phosphorus loads in *F. fabula* (Table 1).

3.5 Scanning *t*-test

Multiple RSs were indicated by the climate and monitoring variables at different periods. Using the climate data (Fig. S8), a positive RS was identified in 1988/89 and 2010 and a negative RS in 1995/96 in the NAO, a positive RS was identified in 1988/89 in the NSE; a negative RS was identified in 1984 and 1989/90 and a positive RS in 1997 in the rain over the German Bight; a positive RS was identified in 1988/89 and in 1997–2000 and a negative RS in 2010 in the SST of the German Bight. In all time series for the Rhine and Maas rivers, two negative RSs were identified, in 1988/89 and 2003/2004 (Fig. S9). Among the RSs detected using the monitoring data (Figs. S10–S12) were a positive RS in 1989/90 based on the SST and SSS, and a negative RS in 2008–2010 based on SSS. According to the nutrient data, the ammonium time series showed a positive RS in 2007–2008; the nitrite data showed two negative RSs, around 1990 and 1993; the nitrate data showed three negative RSs, around 1990, 1995, and 2009; the phosphate data showed two negative RSs, around 1990 and 2000; and the silicate data showed a negative RS in 1989/90. The Chl-*a* observations indicated a negative RS in 2004-2005 and a positive RS in 2009/10. The SPM time series revealed a negative RS in 1989/90 and two positive RSs, in 1993–1997 and 2010/11.

The time series of the abundance and biomass of *Magelona* spp. and *F. fabula* (Fig. S13) differed in their signals. For *Magelona* spp., BRS signals based on abundance appeared in 1985, 1988, and 2010, and based on biomass in 1998. For *F. fabula*, BRS signals based on abundance occurred in 1988, 2000, and 2010, and based on biomass in 1984 and 1988. The time series of benthic abundance, biomass and species numbers (Fig. 7) showed common signals of BRS in 1988/89 with respect to biomass and species number, around 2000 for all time series, and around 2010 for total

abundance and biomass. Surprisingly, no BRS was detected in 2003/2004, when a clear CRS occurred as evidenced by the cumulative runoff (Fig. S2), in the scanning *t*-tests of the River Rhine/Mass time series, and in the precipitation pattern (Fig. 5). These results implied that not every identified CRS drives a BRS, especially in the case of precipitation.

The scanning *t*–test of the macrofauna time series (Fig. 7) identified common BRS signals in 1988/1989, a CRS and BRS around 2000, previously reported in Dippner et al. (2014), and a RS around 2010, noted by Kröncke et al. (2019). Three RSs in the drivers and in the benthic responses were also identified in a scanning *t*-test; these delineated four regimes: 1978–1988 (R1), 1989–2000 (R2), 2001–2009 (R3), and 2010–2017 (R4) and the characteristic feature of the identified RSs were displayed in Table 3. These are considered in the following analyses to identify the impact of RSs on nitrogen source, TP, and isotopic FD.

3.6 Layman model

One result of the Layman model (Layman et al., 2007) is the stable isotope bi-plot of the corrected carbon and nitrogen isotope values, the corresponding convex hulls, and the relative biomass both for all data and for the standardized data (Fig. 8). Figure 9 shows the same stable isotope bi-plot split into the four regimes. The overall metrics of the Layman model for all data (standardized data) and the four regimes are provided in Table 4 (Table 5).

For all six community-wide metrics of the Layman model, which reflect important aspects of trophic structure, the values obtained for *F. fabula* were approximately twice as large as those for *Magelona* spp., considering all data (Fig. 8; Table 4). The convex hull of *F. fabula* covered an area 2.7 times larger than that of *Magelona* spp., with partial overlap. Considering the convex hulls over the four different regimes (Fig. 9), those of R1 and R2, but not R3 and R4, overlapped, indicating niche formation, changes in the food web, and potentially no competition for food.

Standardization of the isotopic data sets resulted in very similar metrics for *F. fabula* and *Magelona* spp. (Fig. 8; Table 5), although the absolute values of *Magelona* spp. were slightly larger. The convex hulls of the two species were of approximately the same size and showed a pronounced overlap, indicative of food competition. In the standardized data (Fig. S14), there was an overlap across R1–R3, but not for R4.

The changes in the six metrics of the Layman model over the four regimes were generally similar in the standardized and non-standardized data sets (Tables 4 and 5). In most cases, there was a clear decreasing trend in the six metrics that indicated a decrease in the diversity of food sources and an increase in niche diversification. A decrease in total diversity over time was also identified and was used in the computation of the FD for the IFR component. Surprisingly, the mean Euclidean distance (*CD*) and mean nearest neighbor distance (*NND*), both of which are used to compute the FD components IFE and IFD, increased slightly from R1 to R2, i.e., during shift to the warm period of 1989–2000.

3.7 Nitrogen source and trophic position

Both $\delta^{15}N_{Phe}$, as the N source measure $\delta^{15}N$ of the source AA Phe, and TP, as the food web structure measure from the respective best fitting TP model, were identified for *Magelona* spp. and *F. fabula* using the spring samples (except two *F. fabula* samples from November 1990 and December 1990) and plotted for each regime (Fig. 10).

Similar to the bulk $\delta^{15}N$ values (Fig. 4), the conservation-corrected $\delta^{15}N\text{-}Phe_{corr}$ values of *Magelona* spp. did not change much between R1 and R4 (mean of 10.9 ± 0.9‰), while *F. fabula* showed roughly 2‰ lower values in the N source measure during R3 and R4 (mean of 8.3±0.4‰) compared to R1 and R2 (mean of 10.3±0.5‰). Deposit feeder *Magelona* spp. had either congruent (R1 and R2) or on average 3.0‰ higher (R3 and R4) $\delta^{15}N\text{-}Phe_{corr}$ values than suspension feeder *F. fabula*.

As expected, the TP values of suspension-feeding *F. fabula* were significantly lower than those of deposit-feeding, carnivorous *Magelona* spp. (t-test; p=6.12E-4, Fig. 10b). The median TP of *F. fabula* was 2.2 (range from 1.7 to 2.6 with mean±STD of 2.2±0.3; n=13) and that of *Magelona* spp. was 2.7 (range from 2.0 to 3.0 with mean±STD of 2.6±0.3; n=12).

The TP of *F. fabula* decreased between R1 and R3, from a median of 2.5 (omnivory) to 1.9 (herbivory), and stayed low during R4 (median TP of 2.0). The decreased TP of this species correlated directly with $\delta^{15}N$ Phe_{corr} ($p < 0.05$). For *Magelona* spp., relatively high median TP values (2.7–2.8) were maintained during R1, R2, and R4, but the median TP during R3 was lower (2.3).

3.8 Environmental controls of food web structure

Significant relationships were mainly found for the bivalve. Those variables related to nutrient availability tended to correlate the strongest and, in all cases, directly with the N-source measure (Fig. S15). Interestingly, there was a three or six–month lag for the relationships in *F. fabula*. Specifically, correlation of nutrient variables such as nitrite or phosphate was strongest with values integrated over the previous three months (Fig. S15b,c). For salinity, it was six months (Fig. S15a).

Among the environmental variables assessed in the correlation analysis, only SSS correlated directly with the TPs of *F. fabula* and *Magelona* spp. (Fig. S16). For both species, the strongest correlations were with the integrated values of the previous 9 months (r^2 for *F. fabula*: 0.57; *Magelona* spp.: 0.53). No further correlation with TP was found for the polychaete; for the bivalve, NO_2^- and PO_4^{3-} correlated directly with TP (r^2 = 0.77, Fig. S16). Chl-*a* and SPM, showed no correlation with TP or $\delta^{15}N_{Phe}$ (not shown).

3.9 Functional diversity

The minimum total area *TA* served as a proxy for IFR, the mean nearest neighbor distance as a proxy for IFE, and the mean Euclidean distance to the centroid *CD* as a proxy for IFD. Figure 11 shows the change in FD for the four identified regimes for

both species in the isotopic FD space, which can be drawn in a 3-D perspective plot because IFR, IFE, and IFD are orthogonal (Mason et al., 2005).

Results for standardized isotopic data (Fig. S17) showed high values in the three isotopic components for *Magelona* spp. and *F. fabula*, occurred during R1 and R2. For *Magelona* spp., the values were intermediate during R3 and low during R4 whereas for *F. fabula* the values of all isotopic components decreased during R3 and R4 (Fig. 11). The decreases in all three isotopic components over time were striking. The same results were obtained for the standardized values resulted in similar patterns (Fig. S17).

3.10 Ecological memory

The de-correlation times of the different time series (Table 2) formed three different clusters: a de-correlation time of 1.2–3.1 months in the climate time series, of 5–6.7 month in the runoff data, and an ecological memory in the biomass time series of 2.6–3.3 years. The short de-correlation time in the climate time series can be attributed to the phase lag between winter climate and spring macrofauna. The de-correlation time in the runoff time series reflected the travel time of water masses from the mouth of the Rhine and Maas rivers into the southern North Sea. The ecological memory of ~3 years in the benthic biomass time series was more complex and required a detailed analysis. This was achieved by using the time series of total abundance, biomass, and species numbers (Fig. S7) to construct low-frequency (LF) and high-frequency (HF) benthic time series. LF time series were obtained by low-pass filtering using a cutoff period of 5 years, and HF time series by subtracting the LF time series from the time series itself (Fig. 12). The obtained LF part was equivalent to the identified regimes and the trendless HF part to a 3-years memory of the system.

4. Discussion

4.1 Isotopic correction

Previous studies have shown that differences between preserved and control samples can be attributed to a decrease in $\delta^{13}C$ values following formalin preservation and an increase in $\delta^{13}C$ values following ethanol preservation (Park & Epstein, 1961; Kaehler & Pakhomov, 2001; Edwards et al., 2002; Rennie et al., 2012; Gonzalez–Bergonzoni et al., 2015). Syväranta et al. (2011) showed that even freezing had a significant impact on the $\delta^{13}C$ and $\delta^{15}N$ values of the Asiatic clam *Corbicula fluminea*. As in our own study, the effects were greater on the carbon isotope than on the nitrogen isotope values. Corrected bulk and AA isotope values were therefore used in all of our analyses (Umbricht et al., 2018).

4.2 Temporal variability of isotope signatures

Magelona spp. and *F. fabula* are recognized as interface feeders, feeding on deposits on the sediment surface or in the water column above the sediment. Magelonids have been primarily described as surface deposit feeders (Jones, 1968; Uebelacker & Jones, 1984). *M. johnstoni* was shown to be a suspension feeder (Fiege et al. 2000, Mortimer & Mackie, 2014), but Jumars et al. (2015) found that carnivory is more common within the family than previously described. *F. fabula* has primarily been described as a suspension feeder, as also indicated by our data.

The similarity in the isotopic signatures of *Magelona* spp. and *F. fabula* suggested similar feeding types, consistent with the shared habitat of these two species, in front of the island of Norderney. Their similar N isotope signatures during the 1980s and 1990s suggested similar food sources. A higher percentage of fertilizer-derived N (Figs. S2 and S3) likely from riverine input/land derived sources may be the reason for the higher $\delta^{15}N$ values of *F. fabula* in the 1980s, as also described in other environments (McClelland et al., 1997). Overall ecosystem functioning seems to be affected by eutrophication via a reduction in sedimenting phytoplankton quality that negatively affected the abundance of the macrozoobenthos key species *F. fabula* with currently unknown effects on sediment biogeochemistry and demersal fish species preying on this bivalve. Further, it is a testable hypothesis that this mechanism may also explain decreases in abundance of other macrozoobenthos key species like *Crangon crangon* (ICES 2023). Nonetheless, the BRS showed changes in feeding behaviors and food sources (Fig. 10). Both species live buried in the sediment and access their food sources using their tentacles (*Magelona* spp.) or siphons (*F. fabula*). De-eutrophication of the North Sea after the 1990s, described in van Beusekom et al. (2019), led to reductions in anthropogenic riverine nutrient loads with lower N isotope values and thus to a separation in the N signatures of the two species.

The change in the isotopic signature of nitrate inputs was reflected in the food base, plankton. In parallel with the nutrient decrease, the $\delta^{15}N$ value presumably also changed, reflected in the $\delta^{15}N$ values of *F. fabula* (Fig. 4). However, the food supply itself is also likely to have decreased, triggering different, species-specific adaptation strategies. These were evidenced by the significant changes in the isotopic signatures and Phe values of the two species, suggesting different diets. Thus, for *F. fabula*, the

lower N values may have been related to the lower N fractions in SPM, and the continuous increases in abundance and biomass to the fact that the bivalve is able to react immediately to spring blooms, which allowed it to use the fresh N material and thus access a food source 3 months earlier than *Magelona* spp. Following de-eutrophication, the ability of *F. fabula* to increase the length of its siphons and thereby access the water column under food limitation (Salzwedel 1979) would have enabled adaptation to the decrease in food availability.

Later, the species of phytoplankton using the excess N or the strong microbial loop thriving on the decaying phytoplankton biomass in eutrophic systems seemed to have produced poor-quality food for *F. fabula*, explaining the latter‘s subsequent low biomass**.** Thus, investing in growth may require better, more appropriate food sources. However, after de-eutrophication, while phytoplankton biomass was low, the food quality was closer to the optimal of *F. fabula*, which due to its earlier adaptation and farther reach was able to more rapidly fulfill its nutritional requirements, investing the nutrients from excess food in growth.

The isotope signature of *Magelona* spp. did not change over time, suggesting that the polychaete's diet, which consists of detritus and small animals (lower C^{13} values compared to *F. fabula*), remained the same before and after de-eutrophication (Mortimer & Mackie, 2014; Mills & Mortimer, 2019). Overall, our isotope data well demonstrate the responses of species to changes in their environment and the potential of those changes to trigger adaptive behaviors.

4.3 Statistical downscaling, events and regime shifts

The time series (Figs. S1–S7) indicated various forms of inter-decadal variability, such as single events, long term trends, and abrupt RSs. An event identified by the changes in SSS and the NH_4 concentration (Fig. S3) was the huge flood of the Elbe River in 2002 (Nies et al., 2003). Another event was the appearance of the extremely cold winter of 1995/96, identified by downscaling of the regional monitoring data using the benthic data (Fig. 6d, e).

The long-term trends identified in the cumulative runoff data of the Rhine and Maas rivers (Fig. S2) were related to the change in precipitation patterns (Fig. 5) and to the consistent downward trends in the nutrient concentrations in the river following the construction of wastewater treatment plants (van Beusekom et al. 2019). As the inter-annual variability in precipitation plays a role in the discharge of the Rhine and Maas rivers, both signals, i.e., the decreasing nutrient concentrations and the precipitation patterns, characterized the long-term trend.

In contrast to other studies (Clare et al., 2017; van Beusekom et al. 2019), for all downscaling combinations there were no correlations with Chl-*a*. Van Beusekom et al. (2019) reported clear regional differences in the Chl-*a* concentrations in the southern and northern Wadden Sea and a strong correlation between summer Chl-*a* (May–September means) and autumn $NH_4 + NO_2^-$ (September–November means). A possible reason for the difference compared to our results is that only benthos data from the spring were used in this study, whereas van Beusekom et al. (2019) included data with different means and representing different time lags in their computations.

Clare et al. (2017) analyzed 40 years of benthic monitoring observations (1972–2012) at the Northumberland coast and concluded that species densities are affected by warming only when food resources are insufficient. In contrast to our results, they found a strong correlation of benthic species with the phytoplankton color index, which increased after the 1988/89 RS due to warming and the increased oceanic inflow from the North Atlantic (Reid et al., 1998; Beaugrand, 2004; McQuatters-Gollop et al., 2007). This result was only partly in accordance with our findings.

Downscaling of the climate predictor to *F. fabula* resulted in a strong correlation of SST with the benthic time series, whereas downscaling of the Norderney monitoring data to both benthic species resulted in a strong correlation with SSS and NO_3^- and a weak correlation of SST with the benthic predictands, in agreement with Clare et al. (2017). However, as mentioned above, in contrast to other studies there were no correlations with Chl-*a*. Two possible reasons for the inconsistency between the findings of Clare et al. (2017) and our results were: 1) unlike our study area, the Northumberland coast is not influenced by major rivers; 2) the species composition differed, as the taxa at the Northumberland coast consisted of equal distributions of deposit feeders, suspension feeders, and predators (Clare et al., 2017), whereas this was not the case at our study site.

A more detailed analysis of climate impacts showed no impact of NAO and rain on the stable isotope data. Rather, the climate predictor was highly correlated with abundance, biomass, and the stable isotopes of carbon and nitrogen (Fig. 6a). The positive correlations of *F. fabula* and the negative correlations of *Magelona* spp. with the discharge and nitrogen transport from the Rhine and Maas rivers, which indicated de-eutrophication, were discussed above (Meyer et al., 2018) and were in agreement with the study by Harley et al. (2006), who concluded that a change in ocean chemistry is more important than a change in temperature for benthic biomass and species composition. Meyer et al. (2019), however, showed that in the near coastal ecosystem of the German Bight, the dominance of functional groups reflects the combined effects of an increasing SST and a regionally decreasing food supply.

As abrupt BRSs were described by non-linear relationships (Scheffer et al., 2001), it was surprising that the BRS in this study was identified by statistical downscaling, which is a linear method. Our results showed that, by integrating multiple drivers, this linear method is also able to predict abrupt non-linear BRSs.

4.4 Layman model

The isotopic space (Fig. 8) constructed with the Layman model can be seen as a multidimensional ecological trait space containing a trophic niche (Newsome et al., 2007). In general, the species distribution in a trait space can be phenotypically overdispersed, random, or clustered (Pausas & Verdu, 2010). Our stable isotope data points in the convex hull (Figs. 8, 9) indicated clustering and clear isotopic differences between the two studied macrofaunal species. Environmental filtering leads to phenotypic clustering, whereas competition results in phenotypic overdispersion (Weiher & Keddy, 1995). The isotopic bi-plot of all data indicated a strong overlap of the convex hulls and thus potential food competition during R1 and

R2. A similar competition between deposit feeders in the Baltic Sea has also been described (Karlson et al., 2015).

However, a comparison of the metrics in the data sets and in the standardized data sets across all four regimes (R1–R4) indicated a decrease in nearly all of them, with the following consequences. 1) The range of $\delta^{15}N$ (*NR*), a measure of the diversity of trophic levels, decreased in the time series of both species but the decrease was more pronounced in *F. fabula*. 2) The range of $\delta^{13}C$ (*CR*) values is a measure of the diversity of consumed food sources (Gonzalez-Bergonzoni et al., 2015). A decrease in *CR* causes niche diversification and a change in the organism's position in the food web. The consequence of decreases in *NR* and *CR* was a decrease in the sizes of the convex hulls, indicating a reduction in the total trophic diversity and the absence of food competition. This was supported by lower ranges of *NR* and *CR* of the four regimes compared with the metrics of all data and the smaller non-overlapping trait spaces (Perry et al., 2002). Our stable isotope results show that *F. fabula* is a suspension or deposit feeder, which is connected to the quality of the plankton. *Magelona´*s stable isotope signature did not change over time, which is a hint that the polychaete feeds on SPM and small and juvenile invertebrates because the C^{13} values are lower as well. Interestingly, our data indicated that the four regimes differed in the competition for food, which is a novel result that was supported by the variability of the isotopic signature (Section 4.2).

4.5 Nitrogen source and trophic position

Bulk $\delta^{15}N$ values covered a range of > 8‰ in *F. fabula* but only 4‰ in *Magelona* spp., consistent with differences in their diets. *F. fabula* species directly filters plankton from the water column and its $\delta^{15}N$ values were those typical of a decline in $\delta^{15}N$ with decreasing nitrogen loads from fertilizers (McClelland et al. 1997; Voss et al., 2006). *F. fabula* shows a decrease of the N source proxy $\delta^{15}N_{Phe}$ by 2‰ over the R1 to R3, while *Magelona* spp. kept similar $\delta^{15}N_{Phe}$ values (Fig. 10a). The source AA $\delta^{15}N_{Phe}$ was presumably more sensitive than the bulk values and underline the robustness of the pattern. Both trends in *F. fabula* are consistent with the decline of total nitrogen, caused by nutrient reduction (van Beusekom et al., 2019). During R4, this de-eutrophication trend seemed to pause or even reverse, as the $\delta^{15}N_{Phe}$ values indicated increasing eutrophication.

By contrast, *Magelona* spp. feeds on sediment surface detritus and small and juvenile invertebrates (Jones, 1968; Uebelacker & Jones, 1984; Fiege et al. 2000; Mortimer & Mackie, 2014; Jumars et al. 2015), food sources with almost constant isotope values, such that there was much less variability in its $\delta^{15}N$ values. The higher $\delta^{15}N_{Phe}$ values of *Magelona* spp. than of *F. fabula* may have reflected higher $\delta^{15}N$ source signal values in surface and subsurface sediments and small animals than in suspended particles, as indicated by the slightly enriched $\delta^{15}N$ values (Macko et al., 1993).

The change in N sources was accompanied by a significant decrease in the TP of *F. fabula*, from a 2.5 to 2.0, attributable to the lower amounts of source isotopes in nitrate. Our TP estimates agreed with the narrow ranges of feeding types that characterize *F. fabula* vs. the wider range within *Magelona* spp..

De-eutrophication affected *F. fabula* with a time lag of 3 months. While no signal was found for *Magelona* spp., the TP of the bivalve decreased by 0.5 TP units, reaching its global mean value of 2.0 in reaction to de-eutrophication. *F. fabula* is thus a robust indicator of the fundamental changes in the benthic food web that occur due to eutrophication and a sensitive indicator of successful nutrient reduction measures, as also noted by Vander Zanden et al. (2003).

Generally, the biomass of organisms decreases as the trophic level increases, attributable to inefficient energy transfer and metabolic costs (Woodson et al., 2018). Any increase in an organism's TP should therefore have pronounced negative consequences for stock productivity, because trophic lengthening directly reduces the efficiency of energy transport to an organism (Paerl, 1988; Mulholland, 2007; Reichle, 2019). At the population level, this implies that if the mean TP of a population increases due to changes in food quality, the productivity and biomass of that population will decrease accordingly (Odum 1960). Conversely, if the mean TP of a population decreases due to de-eutrophication measures, as was the case in this study, then the productivity, abundance, and biomass of that population will increase. Although the secondary production rates of the two species are unknown, the biomass and abundance of *F. fabula* changed directly with the change in its TP (Fig. 13). The decline in abundance and concomitant increase in TP pointed to negative development, because a higher TP does not allow high biomass development. For bivalves and polychaetes, as food sources for fish, sea birds, and other predators, a high biomass is essential for ecosystem functioning.

In summary, de-eutrophication measures in the study area over the last 40 years had a significantly positive impact on the normalization of the TP values of the bivalve *F. fabula*, thus supporting its high biomass. CSIA is an objective method to unambiguously determine the TPs of key species. Monitoring deviations in TP based on the global mean values of sentinel species with strong fluctuations in biomass (for example, in the North Sea, *F. fabula*) can reveal the fundamental changes occurring in ecosystems and the recovery of eutrophication–affected macrofauna. Routine measurements of TP can therefore provide useful information about the success of nutrient reduction measures and guide further management decisions.

4.6 Functional diversity

Biodiversity is often used as an expression of species richness or species abundance (Hooper et al., 2005; Schleuter et al., 2010). It is also linked to the resilience of ecosystem functioning (Oliver et al., 2015), and to a greater resistance of ecosystem productivity (Yachi & Loreau, 1999; Isabell et al., 2015) in response to climate extremes. A loss of habitat and connectivity as well as a BRS impact ecosystem functioning and stability, including by decreasing species diversity (Thompson et al., 2017). However, species richness, as a metric of biodiversity, has several limitations because a reduction in environmental quality can lead to a transient increase in species richness (Hillebrand et al., 2017). Consequently, changes in biodiversity may not be accurately described by trends in species richness; instead, FD may be a better predictor of ecosystem productivity and vulnerability (Tilman et al., 1997; Hulot et al., 2000; Heemsbergen et al., 2004).

Following the approach of Mason et al. (2005) and Villéger et al. (2008), we computed the three isotopic components of FD. Since this approach was originally constructed to unravel the isotopic FD of whole communities over a period of months, care has to be taken for some proxies, as they may not be appropriate for the interpretation of time series data of single species over decades.

On a community level, a decrease in the IFR over the four regimes, as determined for both species and in the original and standardized data sets, would indicate a reduced productivity (Petchey, 2003) and a decreased buffer capacity against environmental fluctuations, such as food sources (Mason et al., 2005). At the species level and thus in this study, however, this interpretation is contradicted by the increased abundance and biomass of both species, with the decrease in IFR instead pointing to habitat stabilization for *F. fabula* and *Magelona* spp. over the last 40 years.

The observed increases in the productivity measures biomass and abundance seemed to have been related to decreases in nutrient concentrations, specifically, nitrogen and phosphorus (van Beusekom et al., 2019). Thus, de-eutrophication might have caused regional differences in macrofaunal community structure due to regional niche separation between the two species, as indicated by the *TA*. These findings, in combination with the identified regional differences in Chl-*a* levels (van Beusekom et al., 2019), may explain the different food web dynamics or trophic pathways and the related reduced resistance to disturbances in the northern Wadden Sea vs. in Jade Bay in the southern Wadden Sea (Baird et al., 2004; 2007; Schückel et al., 2015).

IFE provides information on the biomass distribution of a community in the isotopic functional space. Low values indicate that a community is composed of clusters of species and imply redundancy and food competition. High values can result in a higher productivity, stability, and resilience (Hooper et al., 2005) and occurred during R1 and R2, together with food competition identified in the overlapping convex hulls (Fig. 9). R3 and R4 were characterized by low IFE values, which were related to an enhanced productivity that likely also enhanced stability and resilience. The low IFE values were consistent with the low values obtained for IFR. As noted above, interpretations at the species level differ from those at the community level, as functional biodiversity on the community level mainly stabilizes ecosystem productivity, by increasing resistance to climate events (Isabell et al., 2015). The decrease of all isotopic FD components at the species level over the last 40 years, however, indicated an increase in ecosystem stability and resilience for both species.

IFD provides information on the filling of the isotopic functional space, with high values, such as in R1 and R2, indicating that biomass-dominant species, such as *Magelona* spp. and *F. fabula* (Fig. 3), occupy the isotopic space more densely at its edges (Fig. 9), indicative of trophic specialization and a high degree of niche differentiation (Rigolet et al., 2015). On the species level, this suggests that both species were far away from their optimum niches and likely stressed, which would explain the lower abundance and biomass values during R1 and R2.

Low IFD values, such as during R3 and R4, indicate that biomass is dominated by generalists or that the species are closer to the center of gravity (Fig. 9). This was also indicated by the standardized isotopic time series (Fig. S17). On the species level, this implied that the two species do not have a competition as potentially during R1 and R2; rather, they dominated their optimal respective trophic niche.

The values of all three isotopic functional components, IFR, IFE, and IFD, decreased over time, which can be interpreted as a change in FD due to a BRS. However, in addition to the impacts suggested by the short-term data from whole communities, the consequences of the BRS on the species level included an increased productivity driven by de-eutrophication, a shift in biomass from specialists to generalists, and, after 2000, an increase in the stability and resilience of both species, likely due to niche optimization.

4.7 Ecological memory

Ecological memory has been defined as "the capacity of past states or experiences to influence present or future responses of the community" (Padisak, 1992), as "the degree to which an ecological process is shaped by its past modifications of a landscape" (Peterson, 2002), and as "the ability of the past to influence the present trajectory of ecosystems" (Hughes et al., 2019b). In this study a system memory of 3 years was determined.

An inter-annual variability in biological time series of 3–4 years has been reported for fish stocks (Russell, 1973), at different trophic levels in the North Sea (Steele, 1974), and for zooplankton abundance in the North Atlantic (Taylor, 1995; Taylor & Stephens, 1998), attributed in all cases to a north–south shift of the Gulf Stream.

If the Icelandic Low (IL) pressure is considered as an independent variable, the north–south shift of the Gulf Stream is linked to the east–west shift of the IL, with a lag time of 3 years (Hameed & Piontowski, 2004). The longitudinal position of the IL modifies the southward flow of the Labrador Sea, which influences the northern position of the Gulf Stream, if the position of IL is more easterly. In the case of a more westerly position of the IL, the outflow of the Labrador Sea is suppressed and the North Atlantic Stream is then able to propagate to the north, into the Greenland–Island–Norwegian Sea.

An ecological memory of ~3 years in macrofauna might therefore be due to an internal climate mode with a variability of 2–5 years, driven by atmosphere–ocean interactions in the North Atlantic basin, which had a clearly marked tele-connection (Stephenson et al., 2000). Further time series analyses are necessary to validate this assumption.

5. Conclusion

Abrupt or discontinuous RSs have been the subject of numerous investigations (Smale & Wernberg, 2013; Palmer et al., 2017; van de Pol et al., 2017; Ummenhofer & Meehl, 2017; Turner et al., 2020). In this study, the dynamics of a smooth, linear BRS were revealed by statistical downscaling, although it is a linear method. However, our results indicated that, through a combination of multiple drivers, this linear method is able to predict abrupt non-linear BRSs. A modification of the classification of Scheffer et al. (2001) would therefore be a useful step in improving our understanding of BRSs caused by multiple drivers.

The downscaling experiments and scanning *t*-tests revealed the occurrence of various CRSs and BRSs in different years. Although the composites of precipitation pattern (Fig. 5) and cumulative runoff of the Rhine and Maas rivers (Fig. S2) showed pronounced CRSs, no response could be identified in the benthic time series, indicating that not every CRS causes a BRS. De-eutrophication had a pronounced and positive impact on the two studied species and increased the plasticity of *Magelona* spp..

However, the decreasing trend in river nutrient loads induced a strong response. The BRS in 2000 was caused by a decrease in the TP of *F. fabula*, by a decrease of the diversity of consumed food, indicated by changes in the metrics of the Layman model, and by decreases in vertical biodiversity (Duffy et al. 2007) and total trophic diversity. The absence on an overlap in the convex hulls during R3 and R4 indicated a change in the food web without a potentially food competition between *Magelona* spp. and *F. fabula*. The difference between the isotopic TPs could be attributed to de-eutrophication processes (Meyer et al., 2018; 2019).

In general, coastal communities are well adapted to disturbances (Neumann et al., 2016). However, it is unclear whether inter-annual variability and CRSs can be consistently identified. Magni et al. (2013) found no distinguishable isotope values between bivalves from different ecosystems along the European Atlantic coast. A similar result was obtained by Bremner et al. (2003), in their study of the FD in marine benthic ecosystems in different geographical sectors. By contrast, the biodiversity changes at local scales were shown to often be complex and not easily generalized (Pilotto et al., 2020). In the North Sea (Frelat et al., 2022) and in the northern and southern Wadden Sea in the German Bight, for example, this complexity has been mainly attributed to changes in food web structure (Baird et al., 2004; 2007; Schückel et al., 2015). Other reasons include the impact of invading species (Reise et al., 1999), sea bed degradation (Meyer et al., 2019), and changes in fishing pressure (Silberberger et al., 2018). Therefore, general comparisons of different geographical areas cannot be made and remain a challenge for future research.

The combination of the different methods used in this study offers a useful tool to identify changes in functional biodiversity in response to climate variability, CRSs, and local conditions. Additional investigation of the stable isotope patterns of marine organisms may contribute to accurate determinations of the impact of climate signals on marine functional biodiversity.

Acknowledgement

We thank the captains and crews of the RV "Senckenberg" for their help with sampling throughout the years. We are indebted to numerous colleagues during the last 40 years for technical assistance in sampling, sample processing, biomass determination and taxonomic identification. Anne Breznikar and Jacqueline Umbricht extracted the target organisms from preserved samples, and Jacqueline Umbricht provided a figure, which is greatly acknowledged. We are indebted to Brian Fry for helpful comments and discussions. NCEP re-analysis data were provided by the NOAA/OAR/ESRL PSD, Boulder, Colorado, USA, from their web site at https://www.esrl.noaa.gov/psd/. Time series of riverine discharge as well as total nitrogen and phosphorus loads for the Rhine and Maas rivers are available at https://wiki.cen.uni-hamburg.de/ifm/ECOHAM/__DATA_RIVER. The monitoring time series of Norderney was provided by Justus van Beusekom and is greatly acknowledged. MV and NLW were funded by BluEs (Blue Estuary Project, BMBF, Contract Nr. 03F0864A). The paper is a contribution to the BMBF KüNO3 project "Response of biodiversity change in North Sea food webs mediated by environmental drivers and human activity (BioWeb, 03F0861A).

Authors contribution: JWD performed all computations, except the nitrogen source and trophic position estimations, and wrote the major part of the manuscript. AFC and NLW measured the stable nitrogen isotopes in amino acids. IK conducted the sampling at sea and contributed to the manuscript. IL performed the isotopic analyses. NLW computed the trophic positions, and wrote the sections of the manuscript on trophic position. MV developed the concept and contributed to the text.

Conflict of interest statement: The authors declare that the research was conducted in the absence of any commercial or financial relationships that could be constructed as a potential conflict of interest.

Conflict of interest statement: The authors declare that the research was conducted in the absence of any commercial or financial relationships that could be constructed as a potential conflict of interest.

References

Aebischer NJ, Coulson JC, Colebrook JM (1990) Parallel long-term trends across four marine trophic levels and weather. *Nature*, **347**, 753–755. (doi: 10.1038/347753a0)

Amorim K, Loick-Wilde N, Yuen B, Osvatic JT, Wäge-Recchioni J, Hausmann B, Petersen JM, Fabian J, Wodarg D, Zettler ML (2022) Chemoautotrophy, symbiosis and sedimented diatoms support high biomass of benthic molluscs in the Namibian shelf. *Scientific Reports*, **12(1)**, 9731. (doi:10.1038/s41598-022-13571-w)

Baird D, Asmus H, Asmus R (2007) Trophic dynamics of eight intertidal communities of the Sylt-Rømø Bight ecosystem, northern Wadden Sea. *Marine Ecology Progress Series,* **351**, 25-41. (doi: 10.3354/meps07137)

Baird D, Asmus H, Asmus R (2004) Energy flow of a boreal intertidal ecosystem, the Sylt-Rømø Bight. *Marine Ecology Progress Series,* **279**, 45-61. (doi: 10.3354/meps279045)

Beaugrand G (2004) The North Sea regime shift: evidence, causes, mechanisms and consequences. *Progress in Oceanography,* **60**, 245-262. (doi: 10.1016/j.pocean.2004.02.018)

Beaugrand G *et al.* (2015) Synchronous marine pelagic shifts in the Northern Hemisphere. *Philosophical Transaction of the Royal Society B,* **370**, 20130272 (doi:10.1098/rstb.2013.0272)

Beaugrand G, Kirby RR (2018) How do marine pelagic species respond to climate change? Theories and observations. *Annual Review of Marine Science*, **10**, 169-197. (doi:10.1146/annurev-marine-121916-063304)

Birchenough SNR, et al. (2015) Climate change and marine benthos: a review of existing research and future directions in the North Atlantic. *WIREs climate change*, **6(2)**, 203-223. (https://doi.org/10.1002/wcc.330)

Bosley KL, Wainright SC (1999) Effects of preservatives and acidification on stable isotope ratios (^{15}N:^{14}N, ^{13}C:^{12}C) of two species of marine mammals. *Canadian Journal of Fisheries and Aquatic Sciences,* **56**, 2181-2185. (doi: 10.1023/cjfas-56-11-2181)

Brind'Amour A, Rouyer A, Martin J (2009) Functional gains of including non-commercial epibenthic taxa in coastal beam trawl surveys: A note. *Continental Shelf Research,* **29**, 1189-1194. (doi: 10.1016/j.csr.2009.01.003)

Brind'Amour A, Dubois SF (2013) Isotopic diversity indices: how sensitive to food web structure? *PLoS ONE,* **8(31)**, e84198. (doi:10.1371/journal.pone.0084198)

Bremner J, Rogers SI, Frid CLJ (2003) Assessing functional diversity in marine benthic ecosystems: a comparison of approaches. *Marine Ecology Progress Series*, **254**, 11-25. (doi: 10.3354/meps254011)

Chikaraishi Y, Ogawa NO, Kashiyama Y, Takano Y, Suga H, Tomitani A, Miyashita H, Kitazato H, Ohkouchi N. (2009) Determination of aquatic food-web structure based on compound-specific nitrogen isotopic composition of amino acids. *Limnology and Oceanography: Methods*, **7(11)**, 740-750. (doi: 10.4319/lom.2009.7.740)

Chikaraishi Y, Ogawa NO, Ohkouchi N. (2010) Further evaluation of the trophic level estimation based on nitrogen isotopic composition of amino acids. *Earth, Life, and Isotopes*, **415**, 37-51.

Choi B, Takizawa Y, Chikaraishi Y. (2018) Compression of trophic discrimination in $^{15}N/^{14}N$ within amino acids for herbivorous gastropods. *Researches in Organic Geochemistry*, **34** (2), 29-35. (https://doi.org/10.20612/rog.34.2_29)

Clare DS, Spencer M, Robinson LA, Frid CLJ (2017) Explaining ecological shifts: the role of temperature and primary production in the long-term dynamics of benthic faunal composition. *Oikos*, **126**, 1123-1133. (doi:10.1111/oik.03661)

Collie JS, Richardson K, Steele JH (2004) Regime shifts: can ecological theory illuminate the mechanisms? *Progress in Oceanography,* **60**, 281-302. (doi: 10.1016/j.pocean.2004.02.013)

Conversi A *et al.* (2015) A holistic view of marine regime shifts. *Philosophical Transaction of the Royal Society B,* **370**, 20130279. (http://dx.doi.org/10.1098/rstb.2013.0279)

Cornwell WK, Schwilk DW, Ackerly DD (2006) A trait-based test for habitat filtering: convex hull volume. *Ecology,* **87(6)**, 1465-1471. (doi: 10.1890/0012-9658(2006)87)

De Berg M, Cheong O, van Krevald M, Overmars M (2008) *Computational Geometry. Algorithms and applications*. Springer Verlag, Berlin Heidelberg, 3rd edition, 386pp.

DeNiro MJ, Epstein S (1978) Influence of diet on the distribution of carbon isotopes in animals. *Geochimica et Cosmochimica Acta,* **42**, 495-506. (doi: 10.1016/0016-7037(78)90199-0)

DeNiro MJ, Epstein S (1981) Influence of diet on the distribution of nitrogen isotopes in animals. *Geochimica et Cosmochimica Acta,* **45**, 341-351. (doi: 10.1016/0016-7037(81)90244-1)

de Young B, Harris R, Alheit J, Beaugrand G, Mantua N, Shannon L (2004) Detection regime shifts in the ocean: data considerations. *Progress in Oceanography,* **60**, 143-164. (doi: 10.1016/j.pocean.2004.02.017)

Dippner JW (2006) Future aspects in marine ecosystem modelling. Special WKFDPBI issue. *Journal of Marine Systems,* **61**, 246–267. (doi: 10.1016/j.marsys.2005.06.005)

Dippner JW, Ikauniece A (2001) Long-term zoobenthos variability in the Gulf of Riga in relation to climate variability. *Journal of Marine Systems,* **30**, 155–164. (doi: 10.1016/S0924-7963(01)00055-0)

Dippner JW, Hänninen J, Kuosa H, Vuorinen I (2001) The influence of climate variability on zooplankton abundance in the Northern Baltic Archipelago Sea (SW Finland). *ICES Journal of Marine Science,* **58**, 569-578. (doi: 10.1006/jmsc.2001.1048)

Dippner JW, Kröncke I (2003) Forecast of climate induced change in macrozoobenthos in the southern North Sea in spring. *Climate Research,* **25**, 179–182. (doi: 10.3354/cr025179)

Dippner JW, Kröncke I (2015) Ecological forecasting in presence of abrupt regime shifts. *Journal of Marine Systems,* **150**, 34-40. (doi: 10.1016/j.marsys.2015.05.09)

Dippner JW, Möller C, Kröncke I (2014) Loss of persistence of the North Atlantic Oscillation and its biological implication. *Frontiers in Ecology and Evolution,* **2**, 57. (doi: 10.3389/fevo.2014.00057)

Dippner JW, Fründt B, Hammer C (2019) Lake or Sea? The Unknown Future of Central Baltic Sea Herring. *Frontiers in Ecology and Evololution*, **7**, 143. (doi: 10.3389/fevo.2019.00143)

Dörjes J, Michaelis H, Rhode B (1986) Long-term studies of macro- zoobenthos in the intertidal and shallow subtidal habitats near the island of Norderney (East Frisian coast, Germany). *Hydrobiologia,* **142**, 217–232. (doi: 10.1007/BF00026761)

Drinkwater KF, Belgrano A, Borja A, Conversi A, Edwards M, Greene CH, Ottersen G, Pershing AJ, Walker H (2003) The response of marine ecosystems to climate variability associated with the North Atlantic Oscillation. In: Hurrell, J.W., Kushnir, Y., Ottersen, G., Visbeck, M. (Eds.), *The North Atlantic Oscillation, Climatic Significance and Environmental Impact.* AGU Geophysical Monograph 134, pp. 211–234.

Duffy JE, Cardinale BJ, France KE, McIntyre PB, Thebault E, Loreau M (2007) The functional role of biodiversity in ecosystems: incorporating trophic complexity. *Ecology Letters*, **10**, 522-538. (doi:10.1111/j.1461-0248.2007.01037.x)

Edwards MS, Turner TF, Sharp ZD (2002) Short- and long-term effects of fixation and preservation on stable isotope values ($\delta^{13}C$, $\delta^{15}N$, $\delta^{34}S$) of fluid preserved museum specimen. *Copeia,* **4**, 1106-1112. (https://doi.org/10.1643/0045-8511(2002)002[1106:SALTEO]2.0.CO;2)

Fiege D, Licher F, Mackie ASY (2000) A partial review of the European Magelonidae (Annelida: Polychaeta): *Magelona mirabilis* redefined and *M. johnstoni* sp. nov. distinguished. *Journal of the Marine Biological Association of the United Kingdom* **80(2)**, 215-234. (doi:10.1017/S0025315499001800)

Flynn DFB, Mirotchnick N, Jain M, Palmer MI, Naeem S (2011) Functional and phylogenetic diversity as predictors of biodiversity ecosystem-function relationships. *Ecology*, **92(8)**, 1573-1581. (doi10.2307/23034883)

Frelat R, Kortsch S, Kröncke I, Neumann H, Nordström MC, Olivier PEN, Sell AF (2022) Food web structure and community composition: a comparison across space and time in the North Sea. *Ecography*, e05945. (doi:10/1111/ecog.05945)

Frid CLJ, Garwood PR, Robinson LA (2009) Observing change in a North Sea benthic system: a 33 year time series. *Journal of Marine Systems,* **77(3)**, 227-236 (doi:10.1016/j.jmarsys.2008.01.011)

Fry B (2006) *Stable Isotope Ecology*, Springer, New York, 308pp.

Glibert PM, Burford, MA (2017) Globally changing nutrient loads and harmful algal blooms: Recent advances, new paradigms, and continuing challenges. *Oceanography,* **30**(1), 58–69. (https://doi.org/10.5670/oceanog.2017.110).

Gonzalez-Bergonzoni I, Vidal N, Wang B, Ning D, Liu Z, Jeppesen E, Meerhoff M (2015) General validation of formalin-preserved fish samples in food web studies using stable isotopes. *Methods in Ecology and Evolution,* **6**, 307-314. (doi: 10.1111/2041-210X.12313)

Graham RL (1972) An efficient algorithm for determining the convex hull of a finite planar set. *Information Processing Letters,* **1**, 132-133. (doi: 10.1007/BF02523195)

Hameed S, Piontovski S (2004) The dominant influence of the Islandic Low on the position of the Gulf stream northwall. *Geophysical Research Letter*, **31**, L09303 (doi:10.1029/2004GL019561)

Harley CDG, Hughes AR, Hultgren KM, Miner BG, Sorte CJB, Thornber CS, Rodriguez LF, Tomanek L, Williams SL (2006) The impacts of climate change in costal marine systems. *Ecology Letters*, **9**, 228-241. (doi: 10.1111/j.1461-0248.2005.00871.x)

Hastings A *et al.* (2018) Transient phenomena in ecology. *Science,* **361**, eaat6412. (doi:10.1126/science.aat6412)

Heemsbergen DA, Berg MP, Loreau M, van Hal JR, Faber JH, Verhoef HA (2004) Biodiversity effects on soil processes explained by interspecific functional dissimilarity. *Science*, **306**, 1019. (doi: 10.1126/science.1101865)

Heyen H, Dippner JW (1998) Salinity variability in the German Bight in relation to climate variability. *Tellus,* **50A**, 545–556. (doi:10.1034/j.1600-0879.1998.00012.x)

Hillebrand H *et al.* (2017) Biodiversity change is uncoupled from species richness trends: consequences for conservation and monitoring. *Journal of Applied Ecology*, **55(1),** 1-16. (doi: 10.1111/1365-2664.12959)

Hoeinghaus DJ, Zeug SC, (2008) Can stable isotope ratios provide for community-wide measure of trophic structure? Comment. *Ecology,* **89(8)**, 2353-2357. (https://doi,org/10.1890/07-1143.1)

Hofmann D, Gehre M, Jung K. (2003) Sample preparation techniques for the determination of natural $^{15}N/^{14}N$ variations in amino acids by gas chromatography-combustion-isotope ratio mass spectrometry (GC-C-IRMS). *Isotopes in Environmental and Health Studies*, **39(3)**, 233-244. (doi: 10.1080/1025601031000147630)

Hooper DU *et al.* (2005) Effects of biodiversity on ecosystem functioning: a consensus of current knowledge. *Ecological Monographs*, **75**, 3-35. (https://doi.org/10.1890/04-0922)

Hughes TP *et al*. (2019) Ecological memory modifies the cumulative impact of recurrent climate extremes. *Nature Climate Change*, **9**, 40-43. (doi: 10.1038/s41558-018-0351-2)

Hulot FD, Lacroix G, Lescher–Moutoue FO, Loreau M (2000) Functional diversity governs ecosystem response to nutrient enrichment. *Nature*, **405**, 340-344. (doi:10.1038/35012591)

Hurrell JW (1995) Decadal trends in the North Atlantic Oscillation: regional temperatures and precipitation. *Science,* **269**, 676–679. (doi: 10.1126/science.269.5224.676)

ICES. (2023) Working Group on Crangon Fisheries and Life History (WGCRAN). *ICES Scientific Reports*. **5(93)**, 48 pp. (https://doi.org/10.17895/ices.pub.24220471)

Isabell F *et al*. (2015) Biodiversity increases the resistance of ecosystem productivity to climate extremes. *Nature,* **526**, 574-577. (doi:10.1038/nature15374)

Jackson AL, Inger R, Parnell AC, Bearhop S (2011) Comparing isotope niche width among and within communities: SIBER – Stable Isotope Bayesian Ellipses in R. *Journal of Animal Ecology*, **80**, 595-602. (doi:10.1111/j.13665-2656.2011.01806.x)

Jiang J, Mendelsohn R, Schwing F, Fraedrich K (2002) Coherency detection of multiscale abrupt changes in historic Nile flood levels. *Geophysical Research Letters,* **29(8)**, 112. (doi: 10.1029/2002GL014826)

Jones ML (1968) On the morphology, feeding, and behavior of Magelona sp. *Biological Bulletin* **134**, 272–297. (doi: 10.2307/1539604)

Jumars PA, Dorgan KM, Lindsay SM (2015) Diet of worms emended: an update of polychaete feeding guilds. *Annual Review of Marine Science*, **7**, 497-520. (doi: 10.1146/annrev-marine-010814-020007)

Kaehler S, Pakhomov EA (2001) Effects of storage and preservation in the $\delta^{13}C$ and $\delta^{15}N$ signatures of selected marine organisms. *Marine Ecology Progress Series,* **219**, 299-304. (doi: 10.3354/meps219299)

Kalnay E *et al*. (1996) The NCEP/NCAR Reanalysis 40-year Project. *Bulletin of the American Meteorological Society,* **77**, 437–471. (doi: 10.1175/1520-0477(1996)077<0437)

Karlson AML, Gorokhova E, Elmgren R (2015) Do deposit-feeders compete? Isotopic niche analysis of an invasion in a species-poor system. *Scientific Reports,* **5**, 9715. (doi: 10.1038/srep09715)

Kröncke I (2011) Changes in Dogger Bank macrofauna communities in the 20th century caused by fishing and climate. *Estuarine Coastal and Shelf Science,* **94**, 234–245. (doi: 10.1016/j.ecss.2011.06.015)

Kröncke I, Dippner JW, Heyen H, Zeiss B (1998) Long-term changes in the macrofauna communities off Norderney (East Frisia, Germany) in relation to climate variability. *Marine Ecology Progress Series,* **167**, 25–36. (doi: 10.3354/meps167025)

Kröncke I, Reiss H, Dippner JW (2013) Effects of cold winters and regime shifts on macrofauna communities in shallow coastal regions. *Estuarine Coastal and Shelf Science,* **119**, 79–90. (doi: 10.1016/j.ecss.2012.12.024)

Kröncke I *et al*. (2019) Comparison of common long-term marine ecological trends related to northern hemisphere climate. *Nature Conservation,* **34**, 311-341. (doi: 10.3897/natureconservation.34.30209)

Layman CA, Arrington DA, Montana CC, Post DM (2007) Can stable isotope ratios provide for community-wide measures of trophic structure? *Ecology,* **88(1)**, 42-48. (doi: 10.1890/0012-9658(2007)88<42:)

Layman CA, Post DM (2008) Can stable isotope ratios provide for community-wide measures of trophic structure? Reply. *Ecology,* **89(8)**, 2358-2359. (https/doi.org/10.1890/08-0167.1)

Lenhart H-J, Pätsch J (eds) (2004) Daily loads of nutrients total alkalinity dissolved inorganic carbon, and dissolved organic carbon of the European continental rivers for the years 1977–2002. *Berichte aus dem Zentrum für Meeres- und Klimaforschung. Reihe B: Ozeanographie.* **48**, Springer Verlag, 159pp

Livezey RE (1995) The evaluation of forecast. In: von Storch, H., Navarra, A. (Eds), *Analysis of Climate Variability*. Springer-Verlag, Berlin, 177–196.

Loick-Wilde N, Fernández-Urruzola I, Eglite E, Liskow I, Nausch M, Schulz-Bull D, Mohrholz V. (2019) Stratification, nitrogen fixation, and cyanobacterial bloom stage regulate the planktonic food web structure. *Global Change Biology*, **25(3)**, 794-810. (https://doi.org/10.1111/gbc.14546)

Macko SA, Engel MH, Parker Pl. (1993) Early diagenesis of organic matter in sediments: Assessment of mechanisms and preservation by use of isotopic molecular approaches, in: Engel MH, Macko SH. (Eds.), *Organic Geochemistry*. Plenum Press, New York, pp. 211-224.

Maeda T, Hirose E, Chikaraishi Y, Kawato M, Takishita K, Yoshida T, Verbruggen H, Tanaka J, Shimamura S, Takaki Y, Tsuchiya M, Iwai K, Maruyama T (2012) Algivore or phototroph? Plakobranchus ocellatus (Gastropoda) continuously acquires kleptoplasts and nutrition from multiple algal species in nature. *PLoS ONE*, **7**(7), e42024. (https://doi.org/10.1371/journal.pone.0042023)

Magni P, Rajagopal S, Como S, Jansen JM, van der Velde G, Hummel H (2013) $\delta^{13}C$ and $\delta^{15}N$ variations in organic matter pools, *Mytilus* spp. and *Macoma balthica* along the European Atlantic coast. *Marine Biology,* **160**, 541-552. (doi: 10.1007/s00227-012-2110-7)

Mantua NJ, Hare SR, Zhang Y, Wallace JM, Francis RC (1997) A Pacific interdecadal climate oscillation with impacts on salmon production. *Bulletin of the American Meteorological Society,* **78**, 1069-1080. (doi: 10.1175/1520-0477(1997)078<1069:APICOW>2.0.CO;2)

Mason NWH, Mouillot D, Lee WG, Wilson JG (2005) Functional richness, functional evenness and functional divergence: the primary components of functional diversity. *Oikos*, **111**, 112-118. (https://doi.org/10.1111/j.0030-1299.2005.13886.x)

McClelland JW, Montoya JP (2002) Trophic relationships and the nitrogen isotopic composition of amino acids in plankton. *Ecology*, **83(8)**, 2173-2180. (https://doi.org/10.1890/0012-9658(2002)083[2173:TRATNI]2.0.CO;2)

McClelland J, Valiela I, Michener R. (1997) Nitrogen-stable isotope signatures in estuarine food webs: A record of increasing urbanization in coastal watersheds. *Limnology & Oceanography*, **42(5)**, 930–937. (https://doi.org/10.4319/lo.1997.42.5.0930)

McQuatters-Gollop A, Raitsos DE, Edwards M, Pradhan, Y, Mee LD, Lavender SJ, Attrill MJ (2007) A long-term chlorophyll data set reveals regime shift in North Sea phytoplankton biomass unconnected to nutrient trends. *Limnology and Oceanography*, **52(2)**, 635-648. (https://doi.org/10.4319/lo.2007.52.2.0635)

Meyer J, Kröncke I (2019) Shift in trait-based and taxonomic macrofauna community structure along a 27 year time-series in the south-eastern North Sea. *PLoS ONE*, **14(12)**, e0226410. (doi.org/10.1371/journal.pone.0226410)

Meyer J, Nehmer P, Moll A, Kröncke I (2018) Shifting south-eastern North Sea macrofauna community structure since 1986: A response to de-eutrophication and regional decreasing food supply? *Estuarine, Coastal and Shelf Science*, **213**, 115-127. (doi: 10.1016/j.ecss.2018.08.010)

Meyer J, Nehmer P, Kröncke I (2019) Shifting south-eastern North Sea macrofauna bioturbation potential over the past three decades: a response to increasing SST and regionally decreasing food supply. *Marine Ecology Progress Series*, **609**, 17-32. (doi: 10.3354/meps12802)

Michaelsen, J (1987) Cross-validation in statistical climate forecast models. *Journal of Climate and Applied Meteorology,* **26**, 1589–1600. (doi: 10.1175/1520-0450(1987)026<1589:)

Mills K, Mortimer K (2019) Observations on the tubicolous annelid *Magelona alleni* (Magelonidae), with discussions on the relationship between morphology and behaviour of European magelonids. *Journal of the Marine Biological Association of the United Kingdom* **99**, 715–727. (doi:10.1017/S0025315418000784)

Minagawa M, Wada E (1984) Stepwise enrichment of ^{15}N along food chains: Further evidence and the relation between $\delta^{15}N$ and animal age. *Geochimica et Cosmochimica Acta,* **48**, 1135-1140. (doi: 10.1016/0016-7037(84)90204-7)

Mortimer K, Mackie ASY (2014) Morphology, feeding and behaviour of British *Magelona* (Annelida: Magelonidae), with discussions on the form and function of abdominal lateral pouches. *Memoirs of Museum Victoria* **71**, 177–201. (http://doi.org/10.24199/j.mmv.2014.71.15)

Mouchet MA, Villéger S, Mason NWH, Mouillot D (2010) Functional diversity measures: an overview of their redundancy and their ability to discriminate community assembly rules. *Functional Ecology*, **24**, 867-876 (doi:10.1111/j.1365-2435.2010.01695.x)

Mulholland MR (2007) The fate of nitrogen fixed by diazotrophs in the ocean. *Biogeosciences*, **4**(1), 37-51. (https://doi.org/10.5194/bg-4-37-2007)

Neumann H, Diekmann R, Kröncke I (2016) Functional composition of epifauna in the south-eastern North Sea in relation to habitat characteristics and fishing effort. *Estuarine Coastal and Shelf Science,* **169**, 182–194. (doi: 10.1016/j.ecss.2015.12.011)

Newsome S, Martinez del Rio C, Bearhop S, Phillips DL (2007) A niche for isotope ecology. *Frontiers in Ecology and Environment*, **5**(8), 429-436. (doi:10.1890/060150.01)

Nies H, Gaul H, Oesterreich F, Albrecht H, Schmolke S, Theobald N, Becker G, Schulz A, Frohse A, Dick S, Müller-Navarra S, Herklotz K (2003) Die Auswirkungen des Elbehochwassers vom August 2002 auf die Deutsche Bucht. *Berichte des Bundesamtes für Seeschifffahrt und Hydrographie*, **32**, 81pp. (doi: 10.57802/2z78-tg67)

O'Connell TC (2017) 'Trophic' and 'source' amino acids in trophic estimation: a likely metabolic explanation. *Oecologia*, **184**, 317–326. (https://doi.org/10.1007/s00442-017-3881-9)

Odum HT (1957) Trophic structure and productivity of Silver Springs, Florida. *Ecological Monographs*, **27**(1), 55-112. (https://doi.org/10.2307/1948571)

Ogle K, Barber JJ, Barron-Gafford GA, Bentley LP, Young JM, Huxman TE, Loik ME, Tissue DT (2015) Quantifying ecological memory in plant and ecosystem processes. *Ecology Letters*, **18**, 221-235. (doi:10.1111/ele.12399)

Oliver TH *et al*. (2015) Biodiversity and resilience of ecosystem functions. *Trends in Ecology and Evolution*, **30(11)**, 673-684. (doi:10.1016/j.tree.2015.08.009)

Padisak J (1992) Seasonal succession of phytoplankton in a large shallow lake (Balaton, Hungary) – a dynamic approach to ecological memory, its possible role and mechanism. *Journal of Ecology*, **80**, 217-230. (https:// doi.org/10.2307/2261008)

Paerl HW (1988) Nuisance phytoplankton blooms in coastal, estuarine, and inland waters 1. *Limnology and Oceanography*, **33**(4/2), 823-843. (https://doi.org/10.4319/lo.1988.33.4part2.0823)

Palmer G et al. (2017) Climate change, climate variation and extreme biological response. *Philosophical Transaction of the Royal Society B*, **372**, 20160144. (http://dx.doi.org/10.1098/rstb.2016.0144)

Park R, Epstein S (1961) Metabolic fractionation of C^{13} and C^{12} in plants. *Plant Physiology,* **36(2)**, 133–138. (doi: 10.1104/pp.36.2.133)

Pausas JG, Verdu M (2010) The jungle of methods for evaluationg phenotypic and phylogenetic structure of communities. *BioScience,* **60**, 614-625. (doi: 10.1525/bio.2010.60.8.7)

Perry JN, Liebhold AM, Rosenberg MS, Dungan J, Miriti M, Jakomulska A, Citron-Pousty S (2002) Illustrations and guidelines for selecting statistical methods for quantifying spatial pattern in ecological data. *Ecography,* **25**, 578-600. (doi: 10.1034/j.1600-0587.2002.250507.x)

Pershing AJ, Mills KE, Record NR, Stamieszkin K, Wurtzell KV, Byron CJ, Fitzpatrick D, Golet WJ, Koob E (2015) Evaluating trophic cascades as drivers of regime shifts in different ocean ecosystems. *Philosophical Transaction of the Royal Society B,* **370**, 2013265. (http://doi.org/10.1098/rstb.2013.0265)

Petchey OL (2003) Integrating methods that investigate how complementarity influences ecosystem functioning. *Oikos*, **101**, 323-330. (https:// doi.org/10.1034/j.1600-0706.2003.11828.x)

Petchey OL, Gaston KJ (2002) Extinction and the loss of functional diversity. *Proceedings of the Royal Society London B*, *Biological Science*, **269**, 1721-1727. (https://doi.org/10.1098/rspb.2002.2073)

Petchey OL, O'Gorman EJ, Flynn DFB (2009) A functional guide to functional diversity measures. In: *Biodiversity, Ecosystem Functioning and Human Wellbeing: An Ecological and Economic Perspective*, Chapter 4, 49-59, Oxford University Press. (doi: 10.1093/ac.prof:oso/9780199547951.003.0004)

Peterson BJ, Fry B (1987) Stable Isotopes in ecosystem studies. *Annual Reviews Ecosystems Centers,* **18**, 293-320. (doi: 10.1146/annurev.es.18.110187.001453)

Peterson GD (2002) Contagious disturbances, ecological memory, and the emergence of landscape pattern. *Ecosystem*, **5**, 329-338. (doi:10.1007/s10021-001-0077-1)

Peterson WT, Schwing FB (2003) A new climate regime in the northeast pacific ecosystems. *Geophysical Research Letters,* **30 (17)**, 1896. (doi: 10.1029/2003.GL017528)

Pilotto F *et al*. (2020) Meta-analysis of multidecadal biodiversity trends in Europe. *Nature Communications*, **11**, 3486. (doi.org/10.1038/s41467-020-17171-y)

Podani J, Schmera D (2006) On dendrogram-based measures of functional diversity. *Oikos,* **115**, 179-185. (http://dx.doi.org/10.1111/j.2006.0030-1299.15048.x)

Post DM (2002) Using stable isotopes to estimate trophic position: models, methods and assumptions. *Ecology,* **83**, 703-718. (doi: 10.2307/3071875)

Press WH, Teukolsky SA, Vetterling WA, Flannery BP (1992) *Numerical Recipes. The Art of Scientific Computing.* 2nd Ed, Cambridge University Press 963pp.

Reichle DE (2023) The global carbon cycle and climate change: scaling ecological energetics from organism to the biosphere. Ed. 2, Elsevier. ISBN: 780443187759, 746 pp.

Reid CP, Edwards M, Hunt HG, Warner J (1998) Phytoplankton change in the North Atlantic. *Nature,* **391**, 546. (doi.org/10.1038/35290)

Reid PC, Holliday NP, Smyth TJ (2001) Pulses in the eastern margin current and warmer water off the north west European shelf linked to North Sea ecosystem changes. *Marine Ecology Progress Series,* **215**, 283-287. (doi: 10.3354/meps215283)

Reid PC *et al.* (2016) Global impacts of the 1980s regime shift. *Global Change Biology*, **22**, 682-703 (doi:10.1111/gcb13106)

Reise K, Gollasch S, Wolff WJ (1999) Introduced marine species of the North Sea coasts. *Helgoländer Meeresuntersuchungen*, **52**, 219-234. (https://doi.org/10.1007/BF02908898)

Rennie MD, Ozersky T, Evans DO (2012) Effects of formalin preservation on invertebrate stable isotope values over decadal time series. *Canadian Journal of Zoology,* **90**, 1320-1327. (doi:10.1139/z2012-101)

Rigolet C, Thiebaut E, Brind'Amour A, Dubois SF (2015) Investigating isotopic functional indices to reveal changes in the structure and functioning of benthic communities. *Functional Ecology*, **29**, 1350-1360. (doi:10.1111/1365-2435.12444)

Rocha JC, Peterson G, Bodin Ö, Levin S (2018) Cascading regime shifts within and across scales. *Science,* **362**, 1379-1383. (doi:10.1126/science.aat7850)

Rockström J *et al*. (2009) A safe operating space for humanity. *Nature*, **461**, 472-475. (doi.org/10.1038/461472a)

Rodionov SN (2004) A sequential algorithm for testing climate regime shifts. *Geophysical Research Letters*, **31**, L09204. (doi:10.29/2004GL019448)

Russell FS (1973) A summary of the observations on the occurrence of the planktonic stages of fish off Plymouth 1924–1972. *Journal of Marine Biological Association U.K.*, **53**, 347-355. (doi: 10.1017/S0025315400022311)

Salzwedel H (1979) Zur Ökologie von *Tellina fabula* Gmelin (Bivalvia) in der Deutschen Bucht. Dissertation Christian Albrechts Universität Kiel, 158 pp

Scheffer M, Carpenter S, Foley JA, Folke C, Walker B (2001) Catastrophic shifts in ecosystems. *Nature,* **413**, 591-596. (doi.org/10.1038/35098000)

Schleuter D, Daufresne M, Massol F, Argillier C (2010) A user's guide to functional diversity indices. *Ecological Monographs*, **80(3)**, 469-484. (https://doi.org/10.1890/08-2225.1)

Schönwiese CD (2000) *Praktische Statistik für Meteorologen und Geowissenschaftler, 3rd Edition*, Gebrüder Bornträger, Berlin Stuttgart, 298pp.

Schückel U, Kröncke I, Baird D (2015) Linking long-term changes in trophic structure and function of an intertidal macrobenthic system to eutrophication and climate change using ecological network analysis. *Marine Ecology Progress Series,* **536,** 25-38. (doi: 10.3354/meps536025)

Schwing FB, Jiang J, Mendelsohn R (2003) Coherency of multi-scale abrupt changes between the NAO, NPI, and PDO. *Geophysical Research Letters,* **30(7)**, 1406. (doi: 10.1029/2002GL016535)

Silberberger MJ, Renaud PE, Kröncke I, Reiss H (2018) Food-web structure in four locations along the European shelf indicates spatial differences in ecosystem functioning. *Frontiers in Marine Science*, **5**, 119 (doi: 10.3389/fmars.2018.00119)

Silfer JA, Engel MH, Macko SA, Jumeau EJ. (1991) Stable carbon isotope analysis of amino acid enantiomers by conventional isotope ratio mass spectrometry and combined gas chromatography/isotope ratio mass spectrometry. *Analytical Chemistry*, **63(4)**, 370-374. (http://doi.org/10.1021/ac00004ac014)

Smale DA, Wernberg T (2013) Extreme climate event drives range contraction of habitat–forming species. *Proceedings of the Royal Society B*, **280**, 20122829. (http://dx.doi.org/10.1098/rspb.2012.2829)

Smith MD (2011) An ecological perspective on extreme climatic events: a synthetic definition and framework to guide future research. *Journal of Ecology,* **99**, 656-663. (doi:10.1111/j.1365-2745.2011.01798.x)

Spencer M *et al*. (2011) Temporal change in UK marine communities: trends or regime shifts? *Marine Ecology*, **32** (Suppl. 1), 1-15. (doi:10.1111/j.1439-0485.2010.00422.x)

Steele JH (1974) *The structure of marine ecosystem*. Harvard University Press, Cambridge MA, 128 pp.

Steffen W, Crutzen PJ, McNeill JR (2007) The Anthropocene: are humans now overwhelming the great forces of nature? *AMBIO*, **36(8)**, 614-621. (doi: 10.1579/0044-7447(2007)36[614:TAAHNO]2.0.CO;2)

Stephenson DB, Pavan V, Bojariu R (2000) Is the North Atlantic Oscillation a random walk? *International Journal of Climatology*, **20**, 1-18. (doi.org/10.1002/(SICI)1097-0088(200001)20:1<1::AID-JOC456>3.0.CO;2-P)

Syväranta J, Martino A, Kopp D, Cereghino R, Santoul F (2011) Freezing and chemical preservatives alter the stable isotope values of carbon and nitrogen of the Asiatic clam. (*Corbicula fluminea*). *Hydrobiologia,* **658(1)**, 383-388. (doi: 10.1007/s10750-010-0512-4)

Syväranta J, Lensu A, Marjimäki TJ, Oksanen S, Jones RL (2013) An empirical evaluation of the utility of convex hull and standard ellipse area for assessing population niche widths from stable isotope data. *PLoS ONE,* **8(2)**, e56094. (doi:10.1371/journal.pone.0056094)

Taylor AH (1995) North-South shift of the Gulf Stream and their climatic connection with the abundance of zooplankton in the UK and its surrounding seas. *ICES Journal of Marine Science*, **52**, 711-721. (doi:10.1016/1054-3139(95)80084-0)

Taylor AH, Stephens JA (1998) The North Atlantic Oscillation and the latitude of the Gulf Stream. *Tellus*, **50A**, 134-142. (https://doi.org/10.3402/tellusa.v50i1.14517)

Thompson PL, Rayfield B, Gonzalez A (2017) Loss of habitat and connectivity erodes species diversity, ecosystem functioning, and stability in metacommunity networks. *Ecography*, **40**, 98-108. (doi: 10.1111/ecog.02558)

Tilman D, Knops J, Wedin D, Reich P, Ritchie M, Siemann E (1997) The influence of functional diversity and composition on ecosystem processes. *Science*, **277**, 1300–1302 (doi: 10.1126/science.277.5330.1300)

Turner MG *et al.* (2020) Climate change, ecosystems and abrupt change: science priorities. *Philosophical Transaction of the Royal Society B*, **375**, 20190105. (dx.doi.org/10.1098/rstb.2019.0105)

Uebelacker JM, Jones ML (1984) Family Magelonidae. 7.1– 7.29 in: Uebelacker JM, Johnson PG (eds), Taxonomic guide to the Polychaetes of the Northern Gulf of Mexico. Final report to the Minerals Management Service, contract 14-12-001-29091. Barry A. Vittor & Associates: Mobile, Alabama.

Umbricht J, Dippner JW, Fry B, Kröncke I, Liskow I, Nehmer P, Thoms F, Voss M (2018) Correction of the isotopic composition ($\delta^{13}C$ and $\delta^{15}N$) of preserved Baltic and North Sea macrozoobenthos and their trophic interactions. *Marine Ecology Progress Series,* **595**, 1-13. (https://doi.org/10.3354/meps12543)

Ummenhofer CC, Meehl GA (2017) Extreme weather and climate events with ecological relevance: a review. *Philosophical Transaction of the Royal Society B,* **372**, 20160135. (http://dx.doi.org/10.1098/rstb.2016.0135)

Van Beusekom JEE *et al.* (2019) Wadden Sea Eutrophication: Long-term trends and regional differences. *Frontiers in Marine Science,* **6**, 370. (doi: 10.3389/fmars.2019.00370)

Van de Pol M, Jenouvrier S, Cornelissen JHC, Visser ME (2017) Behavioural, ecological and evolutionary responses to extreme climatic events: challenges and directions. *Philosophical Transaction of the Royal Society B*, **372**, 20160134. (http://dx.doi.org/10.1098/rstb.2016.0134)

Vander Zanden MJ, Casselman JM, Rasmussen JB (1999) Stable isotope evidence for the food web consequences of species invasion in lakes. *Nature,* **401**, 464-467. (doi: 10.1038/46762)

Vander Zanden MJ, Chandra S, Allen BC, Reuter JE, Goldman CR (2003) Historical food web structure and restoration of native aquatic communities in the Lake Tahoe (California-Nevada) Basin. *Ecosystems,* **6**, 274-288. (doi: 10.1007/s10021-002-0204-7)

Veuger B, Middelburg JJ, Boschker HT, Houtekamer M. (2005) Analysis of ^{15}N incorporation into D-alanine: A new method for tracing nitrogen uptake by bacteria. *Limnology and Oceanography: Methods*, **3(5)**, 230-240. (doi:10.4319/lom.2005.3.230)

Villéger S, Mason NWH, Mouillot D (2008) New multidimensional functional diversity indices for a multifaceted framework in functional ecology. *Ecology*, **89**, 2290-2301. (doi: 10.1890/07-1206.1)

Von Storch H, Zorita E, Cubasch U (1993) Downscaling of global climate change estimates to regional scales: an application to Iberian rainfall in wintertime. *Journal of Climate,* **6**, 1161–1171. (doi: 10.1175/ 1520-0442(1993)006<1161:)

Von Storch H, Zwiers F (1999) *Statistical Analysis in Climate Research*. Cambridge Univ. Press, Cambridge, p 116.

Voss M, Deutsch B, Elmgren R, Humborg C, Kuuppo C, Pastuszak M, Rolff C, Schulte U (2006) Source identification of nitrate by means of isotopic tracers in the Baltic Sea catchments. *Biogeosciences*, **3**, 663-676. (https://doi.org/10.5194/bg-3-663-2006)

Wainright SC, Fogarty MJ, Greenfield RC, Fry B (1993) Long-term changes in the Georges Bank food web: trends in stable isotopic composition of fish scales. *Marine Biology*, **115**, 481-493. (https//doi.org/10.1007/BF00349847)

Walker B, Kinzig A, Langridge J (1999) Plant attribute diversity resilience and ecosystem function: the nature and significance of dominant and minor species. *Ecosystem*, **2**, 95-113. (https://doi.org/10.1007/s100219900062)

Weiher E, Keddy PA (1995) The assembly of experimental wetlands plant communities. *Oikos,* **73(3)**, 323-335. (doi: 10.1007/BF03160694)

Winemiller KO (1990) Spatial and temporal variation in tropical fish trophic networks. *Ecological Monographs*, **60**, 331-367. (doi:10.2307/1943061)

Worm B *et al.* (2006) Impacts of Biodiversity Loss on Ocean Ecosystem Services. *Science*, **314**, 787–790. (doi:10.1126/science.1132294)

Woodson C, Schramski JR, Joye SB (2018) A unifying theory for top-heavy ecosystem structure in the ocean. *Nature Communications*, **9**, 23. (doi.org/10.1038/s41467-017-02450-y)

Yachi S, Loreau M (1999) Biodiversity and ecosystem productivity in a fluctuating environment: the insurance hypothesis. *Proceedings of the National Academy of Science*, **96,** 14-1468. (doi: 10.1073/pnas.96.4.1463)

Zhang X, Davidson EA, Mauzerall DL, Searchinger TD, Dumas P, Shen Y (2015) Managing nitrogen for sustainable development. *Nature*, **528**, 51-59. (doi: 10.1038/nature15743)

Zwiers FW, von Storch H (1995) Taking serial correlation into account in tests of the mean. *Journal of Climate,* **8**, 336-351. (doi: 10.1175/ 1520-0442(1995)008<0336:)

Supporting Information

Additional Supporting Information is presented in the online version of this article.

Figure S1: Climate time series

Figure S2: River time series

Figure S3: Monitoring time series Norderney part 1

Figure S4: Monitoring time series Norderney part 2

Figure S5: Abundance and biomass time series of both species

Figure S6: Stable isotope time series

Figure S7: Abundance, biomass, and species number of total macrofauna

Figure S8: Scanning *t*-test of the climate time series

Figure S9: Scanning *t*-test of the river time series

Figure S10: Scanning *t*-test of Norderney monitoring, part 1

Figure S11: Scanning *t*-test of Norderney monitoring, part 2

Figure S12: Scanning *t*-test of Norderney monitoring, part 3

Figure S13: Scanning *t*-tests of the biomass and abundance of both species.

Figure S14: Convex hull and biomass for regimes R1–R4 for the standardized data

Figure S15: Relationship of the N source measure $\delta^{15}N_{Phe}$ (in ‰ vs. N_2) in *F. fabula* with sea surface salinity, nitrite, and phosphate.

Figure S16: Relationship of the TP measures in *F. fabula* and *Magelona* spp. with sea surface salinity, nitrite, and phosphate.

Figure S17: Functional diversity according to the standardized data

Tables

Table 1: Results of downscaling experiments for climate, river, and regional monitoring predictor (RMP) time series and *Magelona* spp. and *F. fabula*. Numbers in parentheses indicate the numbers of considered empirical orthogonal functions in the canonical correlation analysis. North Sea Environmental (NSE) index, sea surface temperature (SST) in the German Bight, discharge (Dis), total nitrogen (TN), and total phosphorus (TP) of the Rhine and Maas rivers (RM), as single predictors, are related to the stable isotope time series. The minus sign in the lag time indicates the number of months (mo) by which the predictand lagged behind the predictor.

Predictor	**Predictand**	**Lag (mo)**	**Correlation**	**Skill**
Climate (4)	*F. fabula* (3)	–2	0.65 ($p<0.01$, N=40)	0.18 ($p<0.01$)
River (2)	*Magelona* spp.(3)	–9	0.60 ($p<0.05$, N=40)	0.17 ($p<0.05$)
River (2)	*F. fabula* (3)	–9	0.62 ($p<0.05$, N=40)	0.38 ($p<0.01$)
RMP (6)	*Magelona* spp.(3)	0	0.69 ($p<0.05$, N=40)	0.10 ($p<0.05$)
RMP (6)	*F. fabula* (3)	0	0.75 ($p<0.01$, N=40)	0.23 ($p<0.05$)
NSE (4)	δ^{13}C *F. fabula*	–2	0.53 ($p<0.05$, N=29)	0.12 ($p<0.05$)
NSE(4)	δ^{15}N *F. fabula*	–2	0.69 ($p<0.01$, N=29)	0.14 ($p<0.01$)
SST	δ^{13}C *F. fabula*	–2	0.52 ($p<0.01$, N=29	0.22 ($p<0.01$)
SST	δ^{15}N *F. fabula*	–2	0.65 ($p<0.05$, N=29)	0.38 ($p<0.01$)
RM Dis	δ^{15}N *Magelona* spp.	–9	0.43 ($p<0.05$, N=30)	0.12 ($p<0.01$)
RM TN	δ^{15}N *Magelona* spp.	–9	0.43 ($p<0.05$, N=30)	0.11 ($p<0.05$)
RM TN	δ^{15}N *F. fabula*	–9	0.42 ($p<0.05$, N=29)	0.12 ($p<0.05$)

RM TP	$\delta^{15}N$ *F. fabula*	–9	0.51 ($p<0.01$, N=29)	0.22 ($p<0.01$)

Table 2: Analysis of ecological memory. The climate time series are the NAO index, the NSE index, precipitation in the catchment, and the SST in the German Bight. The river predictors are the discharge (Dis), total nitrogen (TN), and total phosphorus (TP) of the Rhine and Maas rivers (RM). The biological time series are the biomass of total macrofauna and the biomass of *Magelona* spp. (Mag) and *F. fabula* (Fab). The table shows the lag $\alpha(1)$, the memory of the system expressed as the de-correlation time τ_D (in months [m] or years [y]), and the equivalent sample size (ESS) used in the scanning *t*-test (Zwiers & von Storch, 1995).

Time series	Lag α(1)	Memory	ESS
NAO	**0.21**	**1.52 m**	**316.10**
NSE	**0.31**	**1.89 m**	**253.47**
Rain	**0.11**	**1.24 m**	**388.60**
SST	**0.52**	**3.16 m**	**151.56**
RM Dis_M	**0.74**	**6.65 m**	**72.20**
RM TN_M	**0.74**	**6.58 m**	**72.99**
RM TP_M	**0.67**	**5.08 m**	**94.40**
Biomass (Total)	**0.52**	**3.15 y**	**12.38**
Biomass (Mag)	**0.48**	**2.56 y**	**15.63**
Biomass (Fab)	**0.53**	**3.29 y**	**12.15**

Table 3: Characteristic features of the identified RS based on Figs S1–S2. Displayed were the properties of the anomalies of selected variables: positive (+) and negative (-) anomalies or oscillatory (osc) behavior. ex(NN) means excluding the year NN.

Regime	R1	R2	R3	R4
Period	1978-1988	1989-2000	2001-2009	2010-2017
Temperature	-	osc	+	+
Precipitation	variable	-	mainly -	osc
R/M Discharge	+	- ex(94, 95, 99)	- ex(01, 02)	-
R/M total N	+	- ex(94, 95, 99)	- ex(03)	-
R/M total P	+	- ex(94, 95)	-	-
Surface salinity	-	osc	mainly -	-
NH_4	+	osc	-	osc
NO_2	+	osc	-	-
NO_3	+	osc	osc	-
PO_4	+	osc	-	osc

Table 4: Results of the Layman model applied to all data and to the four regimes (R1: 1978–1988, R2: 1989–2000, R3: 2001–2009, and R4: 2010–2017) for *F. fabula* (**F**) and *Magelona* spp. (**M**). **NR**: $\delta^{15}N$ range of the data, **CR**: $\delta^{13}C$ range of the data, **TA**: total area of all species in the convex hull area, **CD**: mean Euclidean distance to the centroid, **NND**: mean nearest neighbor distance, and **SDNND**: standard deviation of **NND**. The functional diversity (**FD**) properties equivalent to the Layman results are shown in parentheses: isotopic functional richness (**IFR**), isotopic functional divergence (**IFD**) and isotopic functional evenness (**IFE**).

	All data		**1978-1988**		**1989-2000**		**2001-2009**		**2010-2017**	
Metrics (FD properties)	**F**	**M**	**F**	**M**	**F**	**M**	**F**	**M**	**F**	**M**
NR	**7.62**	**3.35**	**4.84**	**3.35**	**6.16**	**2.27**	**1.08**	**2.04**	**1.98**	**1.08**
CR	**4.24**	**3.53**	**3.77**	**2.28**	**3.78**	**2.61**	**2.04**	**1.70**	**2.40**	**1.08**
TA (IFR)	**22.55**	**8.34**	**9.46**	**3.80**	**6.77**	**3.38**	**1.61**	**1.80**	**0.96**	**0.64**
CD (IFD)	**2.01**	**0.95**	**1.88**	**1.00**	**1.85**	**1.10**	**0.75**	**0.76**	**0.76**	**0.47**
NND (IFE)	**2.71**	**1.34**	**2.46**	**1.36**	**2.67**	**1.41**	**0.96**	**1.00**	**1.04**	**0.61**
SDNND	**0.09**	**0.05**	**0.31**	**0.17**	**0.63**	**0.24**	**0.12**	**0.13**	**0.13**	**0.08**

Table 5: Same as Table 4 but for the standardized data.

	All data		1978-1988		1989-2000		2001-2009		2010-2017	
Metrics (FD properties)	**F**	**M**	**F**	**M**	**F**	**M**	**F**	**M**	**F**	**M**
NR	**3.57**	**4.12**	**2.27**	**4.12**	**2.88**	**2.79**	**0.50**	**2.50**	**0.93**	**1.32**
CR	**4.07**	**4.73**	**3.62**	**3.06**	**3.62**	**3.49**	**1.96**	**2.27**	**2.30**	**1.43**
TA (IFR)	**10.12**	**13.71**	**4.26**	**6.28**	**3.02**	**5.55**	**0.72**	**2.94**	**0.42**	**1.04**
CD (IFD)	**1.24**	**1.22**	**1.18**	**1.28**	**1.23**	**1.43**	**0.62**	**0.96**	**0.59**	**0.61**
NND (IFE)	**1.68**	**1.71**	**1.57**	**1.74**	**1.77**	**1.83**	**0.79**	**1.27**	**0.82**	**0.78**
SDNND	**0.06**	**0.06**	**0.20**	**0.22**	**0.35**	**0.30**	**0.10**	**0.16**	**0.10**	**0.10**

List of Figures

Figure 1: Flowchart of the lab methods and mathematical analyses. Lab work: Sample preparation followed by isotope ratio mass spectrometer (IRMS) analysis yielded two isotopic data sets, biological bulk data (BD) and the amino acids (AA) of the species, which served as input data (green boxes) in the analyses. PD: physical data. Yellow circles mark the different models applied: statistical downscaling (SDS), scanning *t*-test (STT), Layman model (LM), trophic position model (TPM), de-correlation time (DCT), and functional diversity model (FDM). PD and BD were the predictor and predictand input data for the SDS model, used for the predictions. The green arrows indicate that all PD and BD time series served as input data in the SDS, STT, and DCT models. Red arrows indicate the influence of different regimes, and pink boxes the final results. The outputs of the FDM are the isotopic functional richness (IFR), a proxy for productivity and buffer capacity; isotopic functional evenness (IFE), a proxy for redundancy and competition; and isotopic functional divergence (IFD), a proxy for trophic specialization and niche differentiation. The light blue boxes mark the results and the intermediate products used in further computations.

Figure 2: Study area and stations sampled from 1978 to 2017 off the island of Norderney in the southern North Sea, marked by a rectangle in the larger map after Kröncke et al. (2013). The inflows of the Rhine and Maas rivers are marked with arrows.

Figure 3: Time series of the abundance (ind m^{-2}) and biomass (mg AFDW m^{-2}) of *Magelona* spp. (a, b) and *F. fabula* (c, d).

Figure 4: Observed (dashed blue line) and corrected (solid red line) time series of the $\delta^{13}C$ values and corresponding $\delta^{15}N$ values for *F. fabula* and *Magelona* spp.. The corrected time series is obtained after the application of correction factor.

Figure 5: Anomalies of the precipitation rate for the periods 1978–1988 (a), 1989–2003 (b) and 2004–2017 (c). Note the different scale in a.

Figure 6a: Results of the downscaling experiments. Top: CCA pattern for predictor (black) and predictand (red). Down: time coefficients of the first CCA. The numbers along the axes are the amount of explained variance in the CCA modes: predictor in black and predictand in red. The predictor–predictand combination is NSE–*F. fabula*.

Figure 6b: Explanation see Figure 6a. The predictor–predictand combination is Rhine/Maas–*Magelona* spp.

Figure 6c: Explanation see Figure 6a. The predictor–predictand combination is Rhine/Maas–*F. fabula*

Figure 6d: Explanation see Figure 6a. The predictor–predictand combination is Norderney monitoring–*Magelona* spp.

Figure 6e: Explanation see Figure 6a. The predictor–predictand combination is Norderney monitoring–*F. fabula*

Figure 7: Scanning *t*-test of the benthos time series for abundance, biomass, and species number. Significant changes are shown in color, negative values in cyan and positive values in magenta.

Figure 8: Stable isotope bi-plot showing the means of the corrected carbon and nitrogen isotope values (upper panel) and their standardized values (lower panel), the corresponding convex hulls, and the relative biomass of *Magelona* spp. (blue) and *F. fabula* (red).

Figure 9: Convex hull and relative biomass of *Magelona* spp. (blue) and *F. fabula* (red) for the four identified regimes (R1–R4) compared with the 40-year data ensemble shown in Figure 8 (dashed lines).

Figure 10: Regime-specific a) stable nitrogen isotope distribution of the N source proxy phenylalanine corrected according to Table 1 ($\delta^{15}N\ Phe_{corr}$ in ‰ vs. N_2); b) trophic position of *Magelona* spp. (blue) and *F. fabula* (red). N=3 for each box whisker plot. Numbers are the median values.

Figure 11: Functional diversity in the four identified regimes for *Magelona* spp. (upper panel) and *F. fabula (*lower panel) in the isotopic functional diversity space constructed from IFR, IFD, and IFE based on the results of the Layman model.

Figure 12: Low-frequency (LF) and high-frequency (HF) benthic time series. LF time series (a) were obtained by low-pass filtering using a cutoff period of 5 years, and HF time series (b) by subtracting the LF time series from the time series itself. The LF part was equivalent to the identified regimes and the trendless HF part to the 3-year memory of the system.

Figure 13: Composite relationships between (a) abundance and (b) biomass vs. the trophic position of *F. fabula*. The exponential regression lines indicate significant relationships between the variables (see the regression equations in the panels).

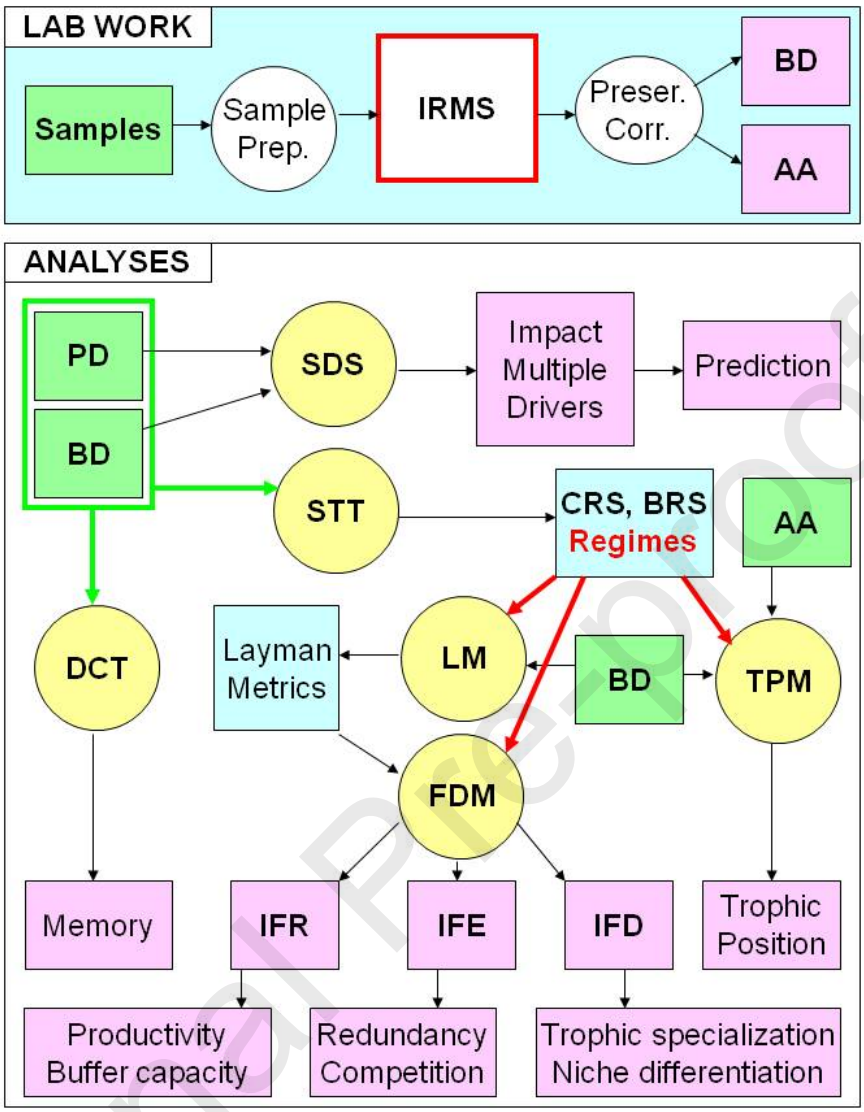

Figure 1: Flowchart of the lab methods and mathematical analyses. Lab work: Sample preparation followed by isotope ratio mass spectrometer (IRMS) analysis yielded two isotopic data sets, biological bulk data (BD) and the amino acids (AA) of the species, which served as input data (green boxes) in the analyses. PD: physical data. Yellow circles mark the different models applied: statistical downscaling (SDS), scanning *t*-test (STT), Layman model (LM), trophic position model (TPM), de-correlation time (DCT), and functional diversity model (FDM). PD and BD were the predictor and predictand input data for the SDS model, used for the predictions. The green arrows indicate that all PD and BD time series served as input data in the SDS, STT, and DCT models. Red arrows indicate the influence of different regimes, and pink boxes the final results. The outputs of the FDM are the isotopic functional richness (IFR), a proxy for productivity and buffer capacity; isotopic functional evenness (IFE), a proxy for redundancy and competition; and isotopic functional divergence (IFD), a proxy for trophic specialization and niche differentiation. The

light blue boxes mark the results and the intermediate products used in further computations.

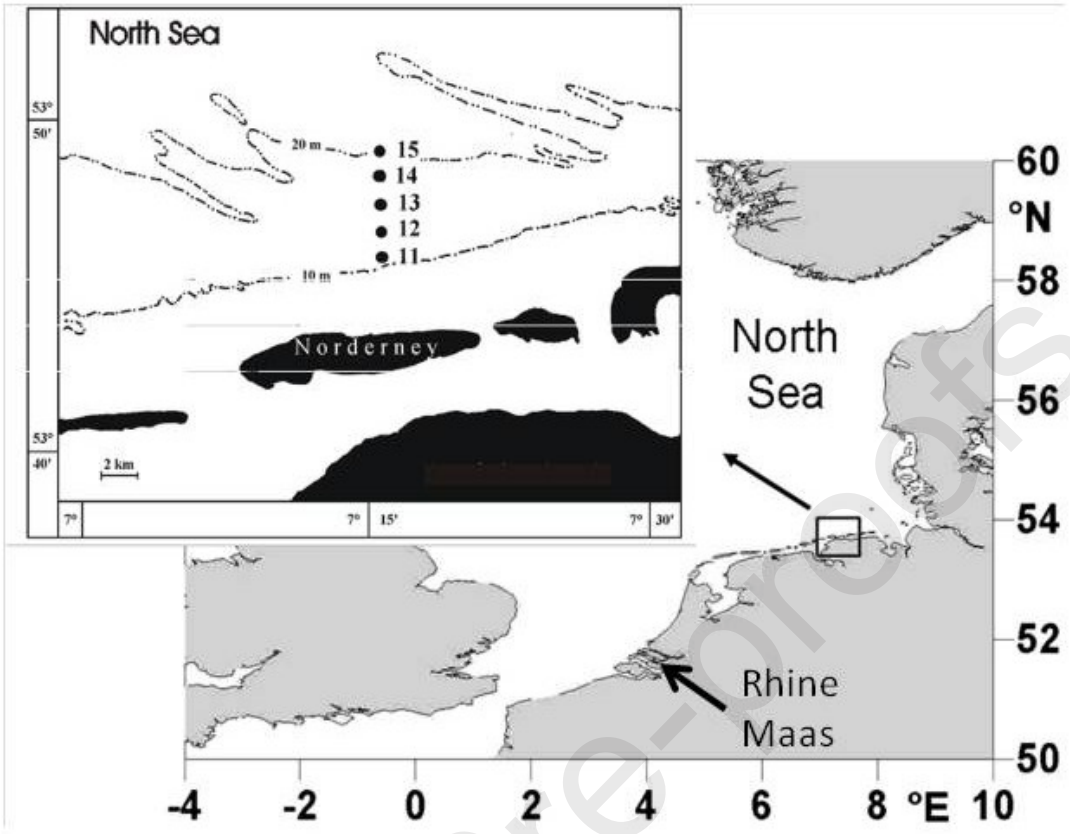

Figure 2: Study area and stations sampled from 1978 to 2017 off the island of Norderney in the southern North Sea, marked by a rectangle in the larger map after Kröncke et al. (2013). The inflows of the Rhine and Maas rivers are marked with arrows.

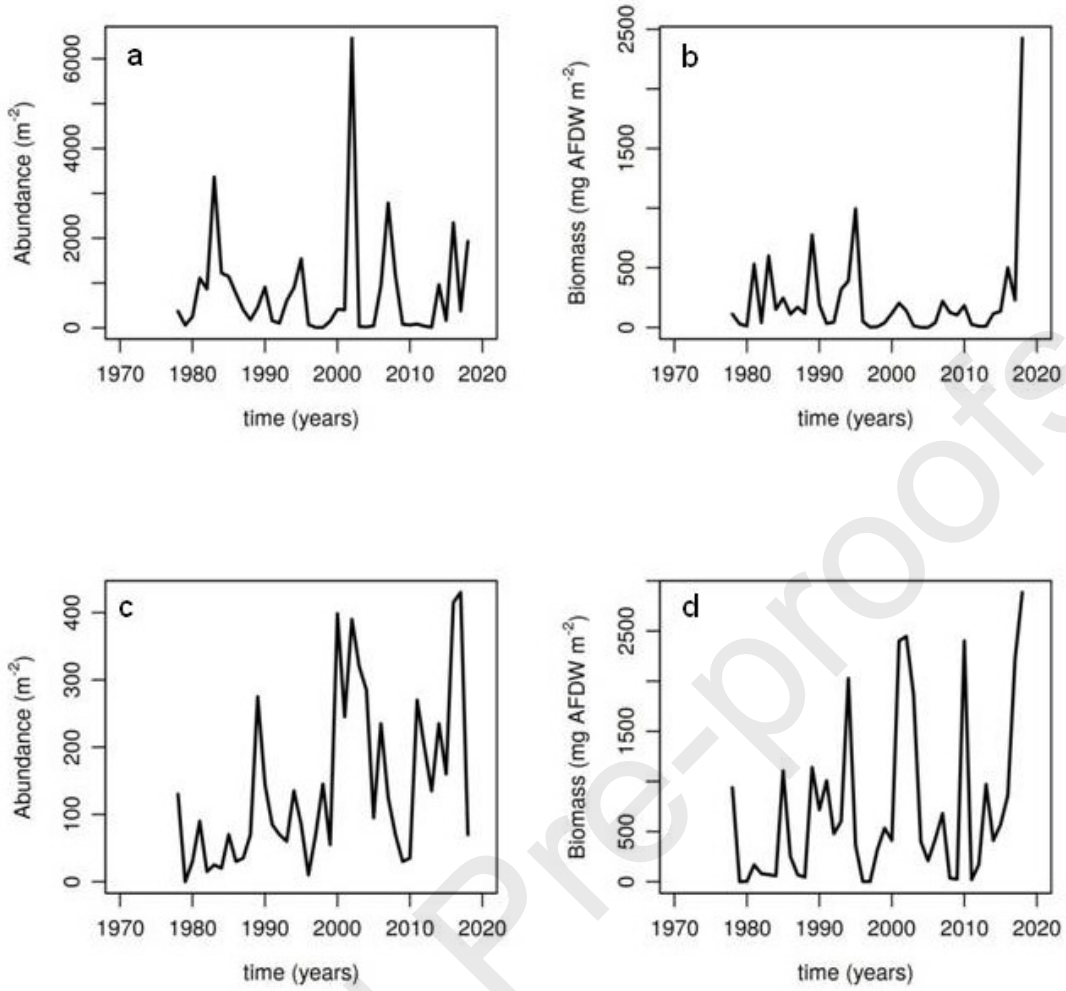

Figure 3: Time series of the abundance (ind m^{-2}) and biomass (mg AFDW m^{-2}) of *Magelona* spp. (a, b) and *F. fabula* (c, d).

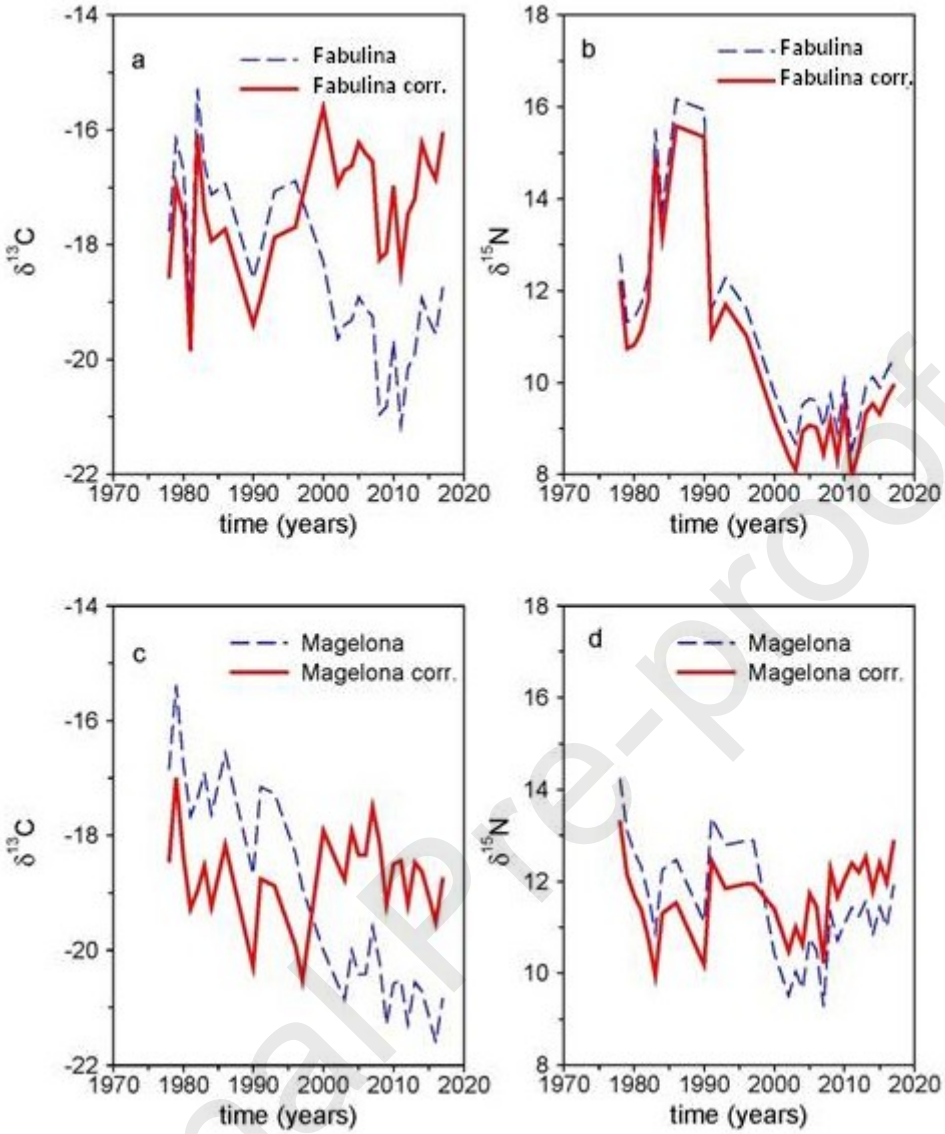

Figure 4: Observed (dashed blue line) and corrected (solid red line) time series of the $\delta^{13}C$ values and corresponding $\delta^{15}N$ values for *F. fabula* and *Magelona* spp.. The corrected time series is obtained after the application of correction factor.

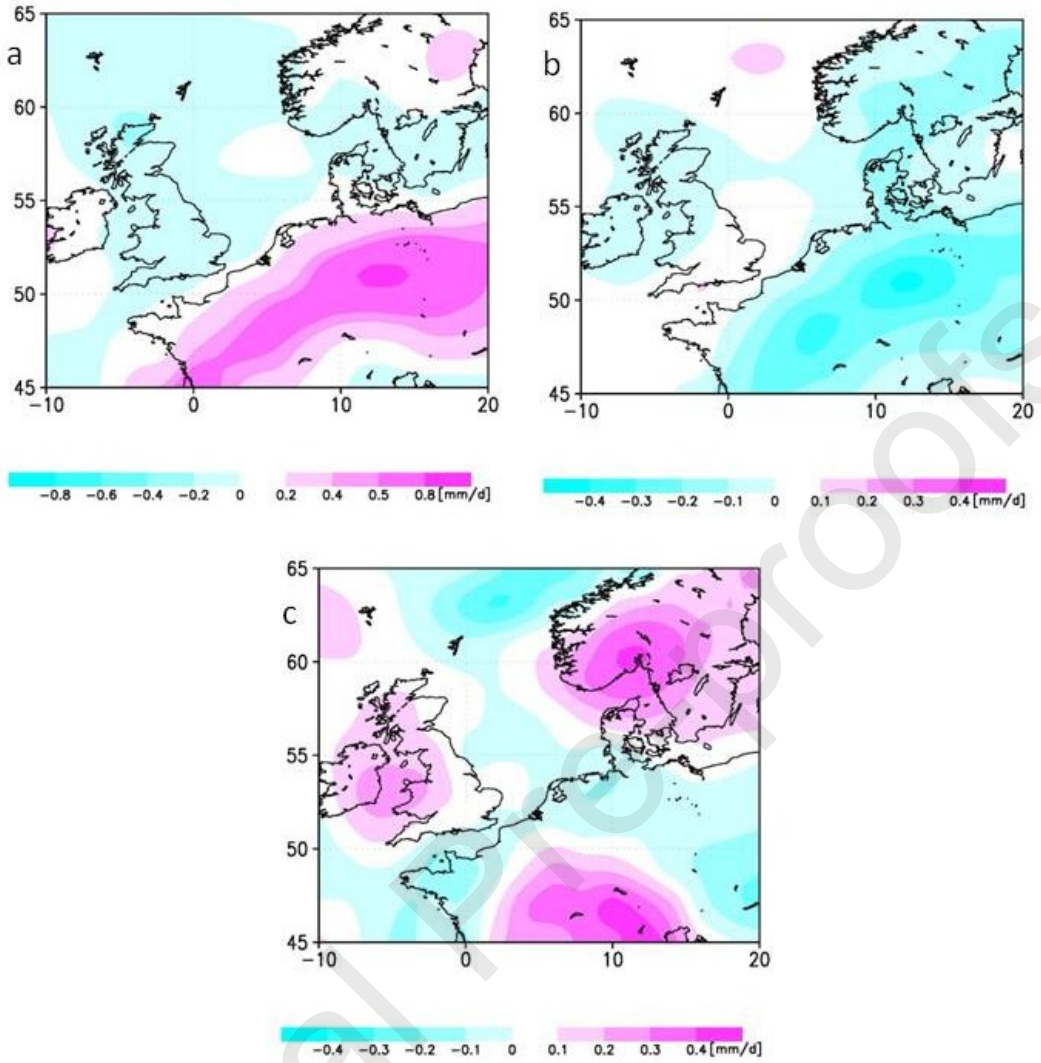

Figure 5: Anomalies of the precipitation rate for the periods 1978–1988 (a), 1989–2003 (b) and 2004–2017 (c). Note the different scale in a.

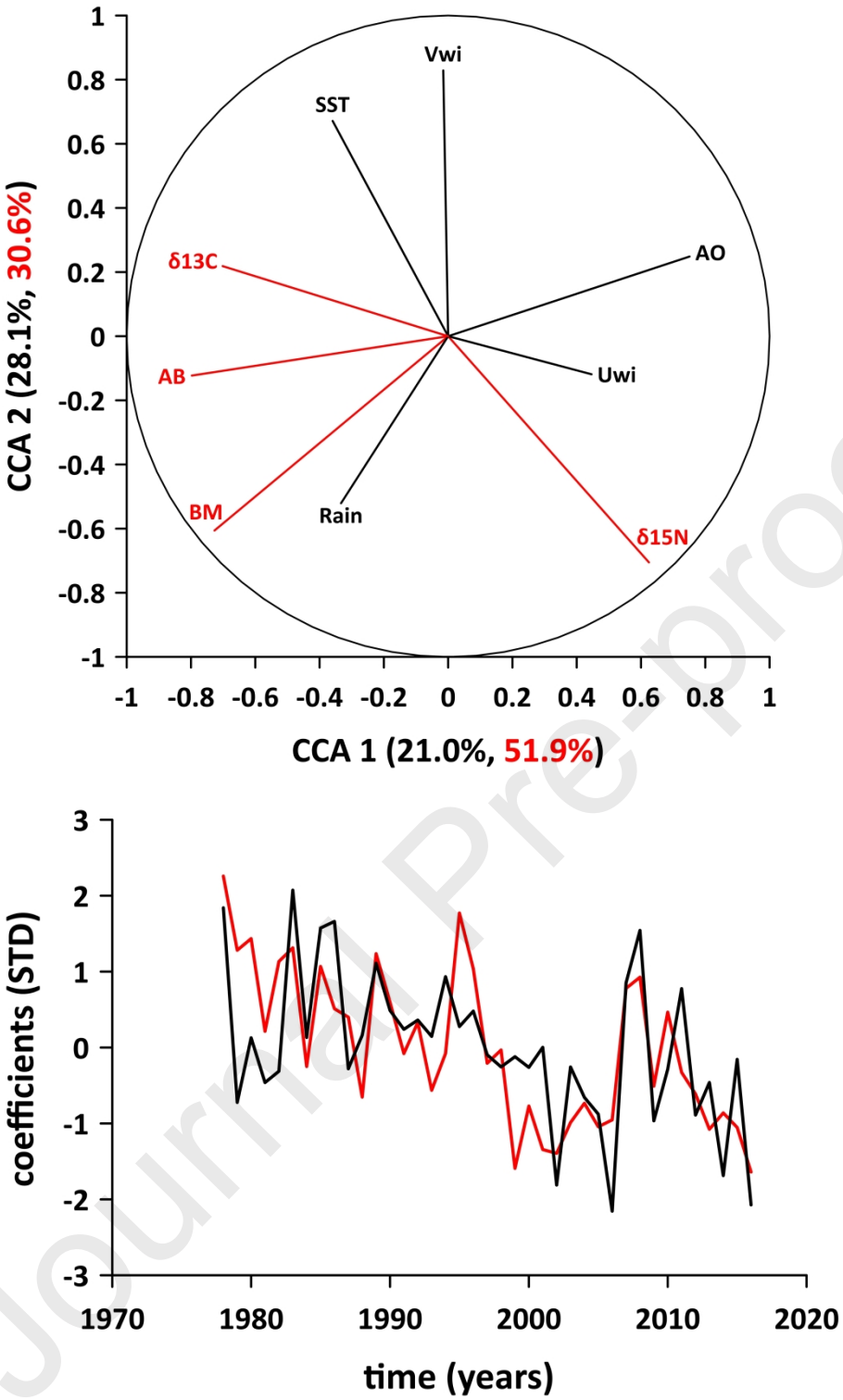

Figure 6a: Results of the downscaling experiments. Top: CCA pattern for predictor (black) and predictand (red). Down: time coefficients of the first CCA. The numbers along the axes are the amount of explained variance in the CCA modes: predictor in black and predictand in red. The predictor–predictand combination is NSE–*F. fabula*.

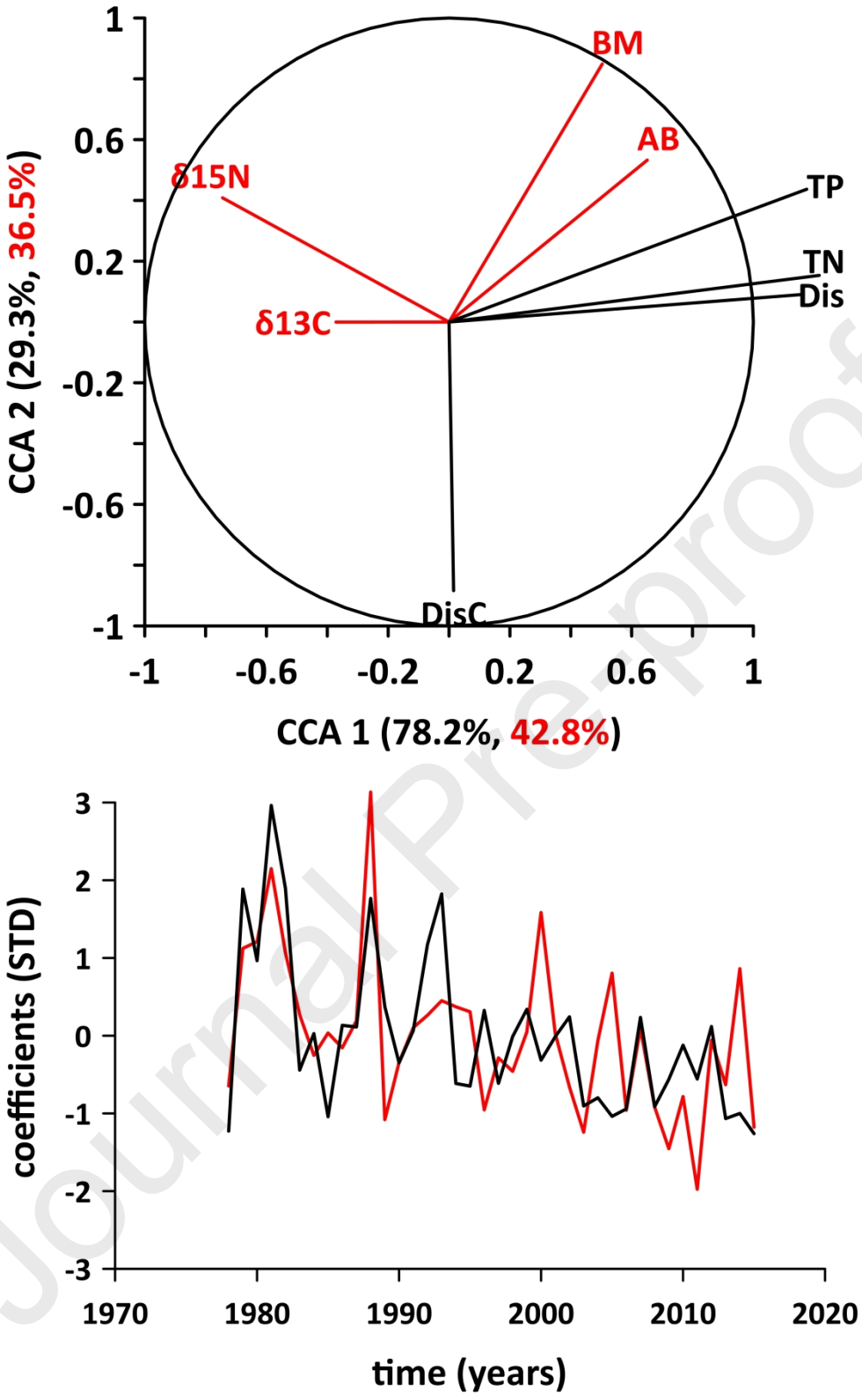

Figure 6b: Explanation see Figure 6a. The predictor–predictand combination is Rhine/Maas–*Magelona* spp.

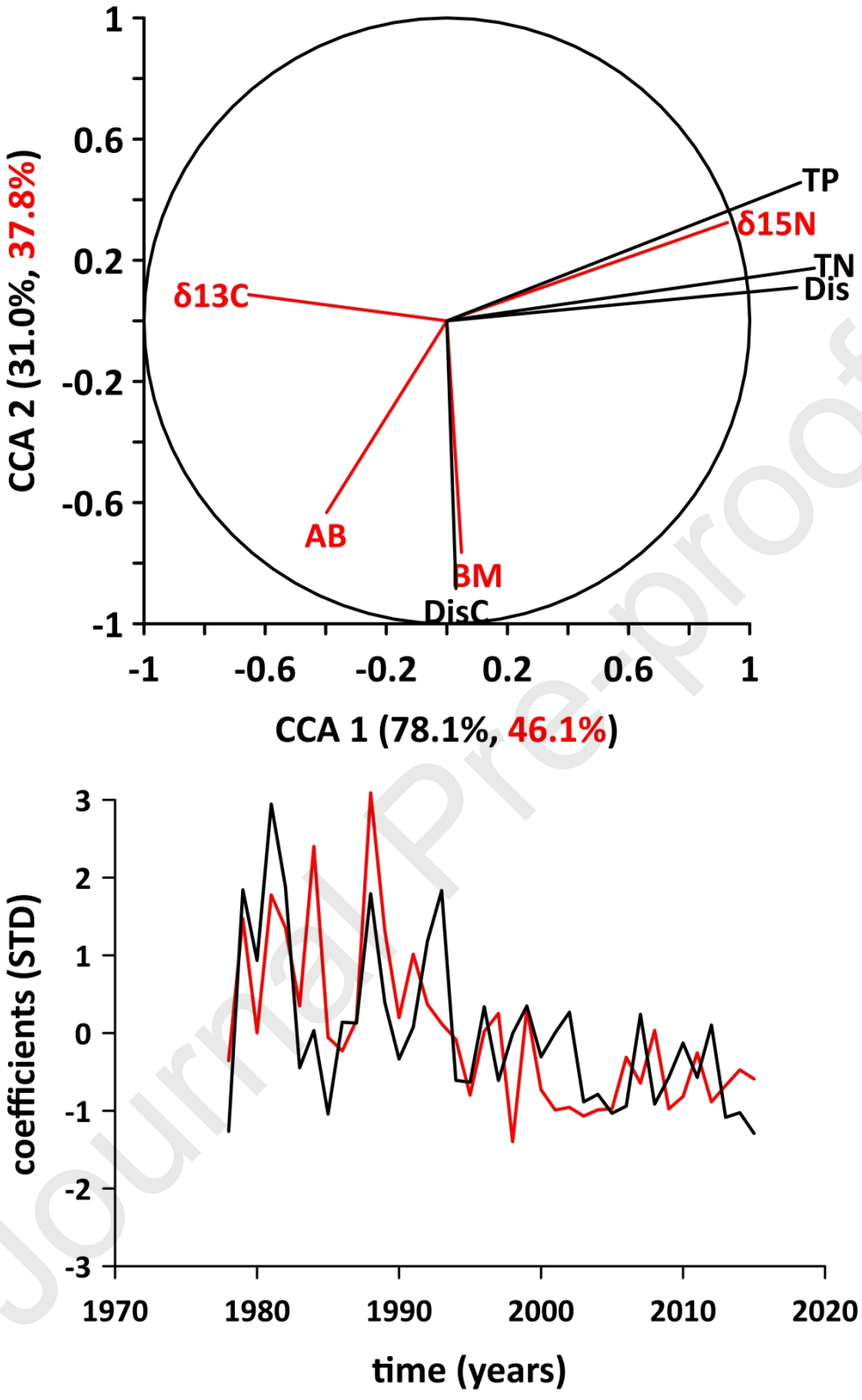

Figure 6c: Explanation see Figure 6a. The predictor–predictand combination is Rhine/Maas–*F. fabula*

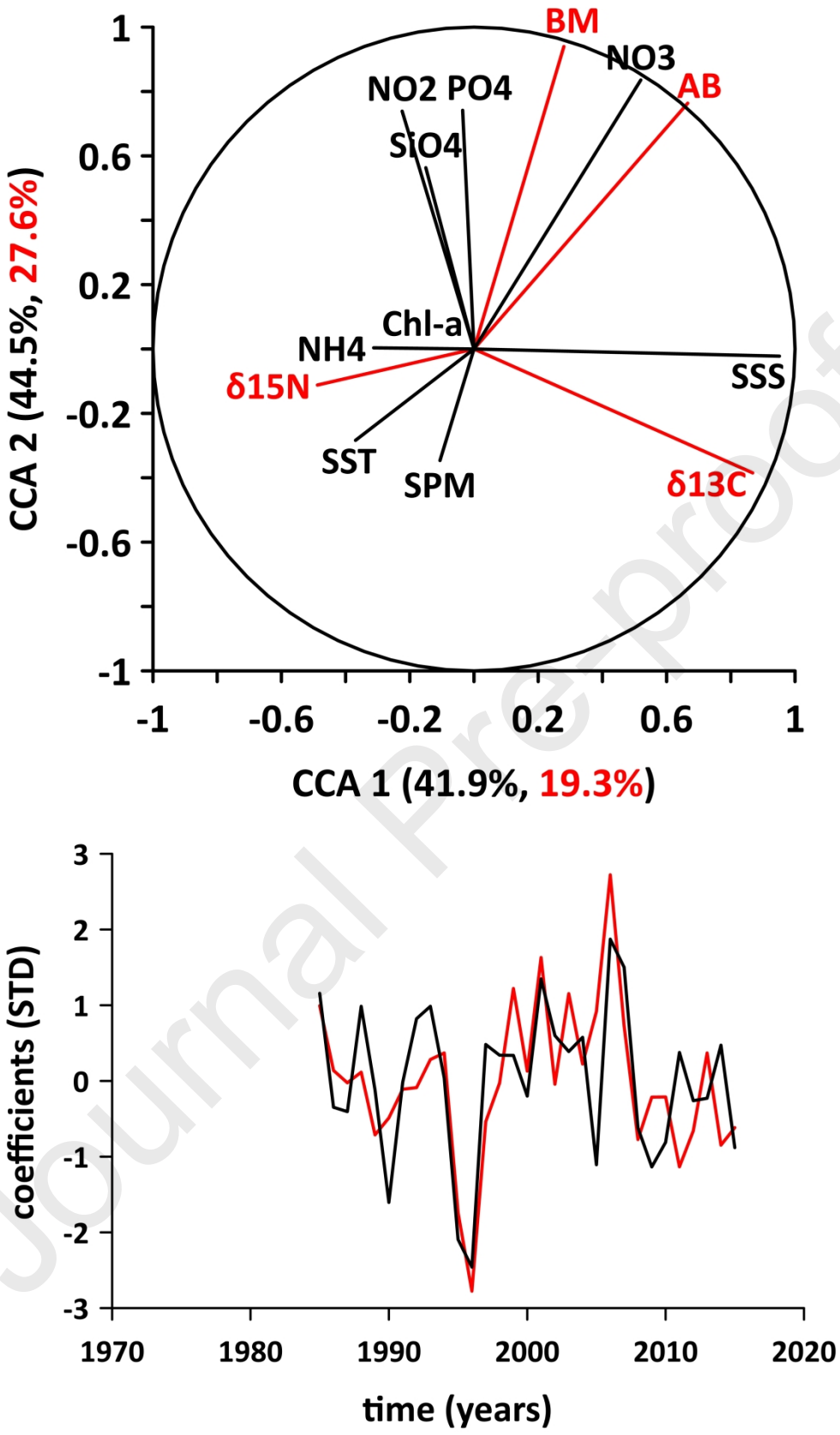

Figure 6d: Explanation see Figure 6a. The predictor–predictand combination is Norderney monitoring–*Magelona* spp.

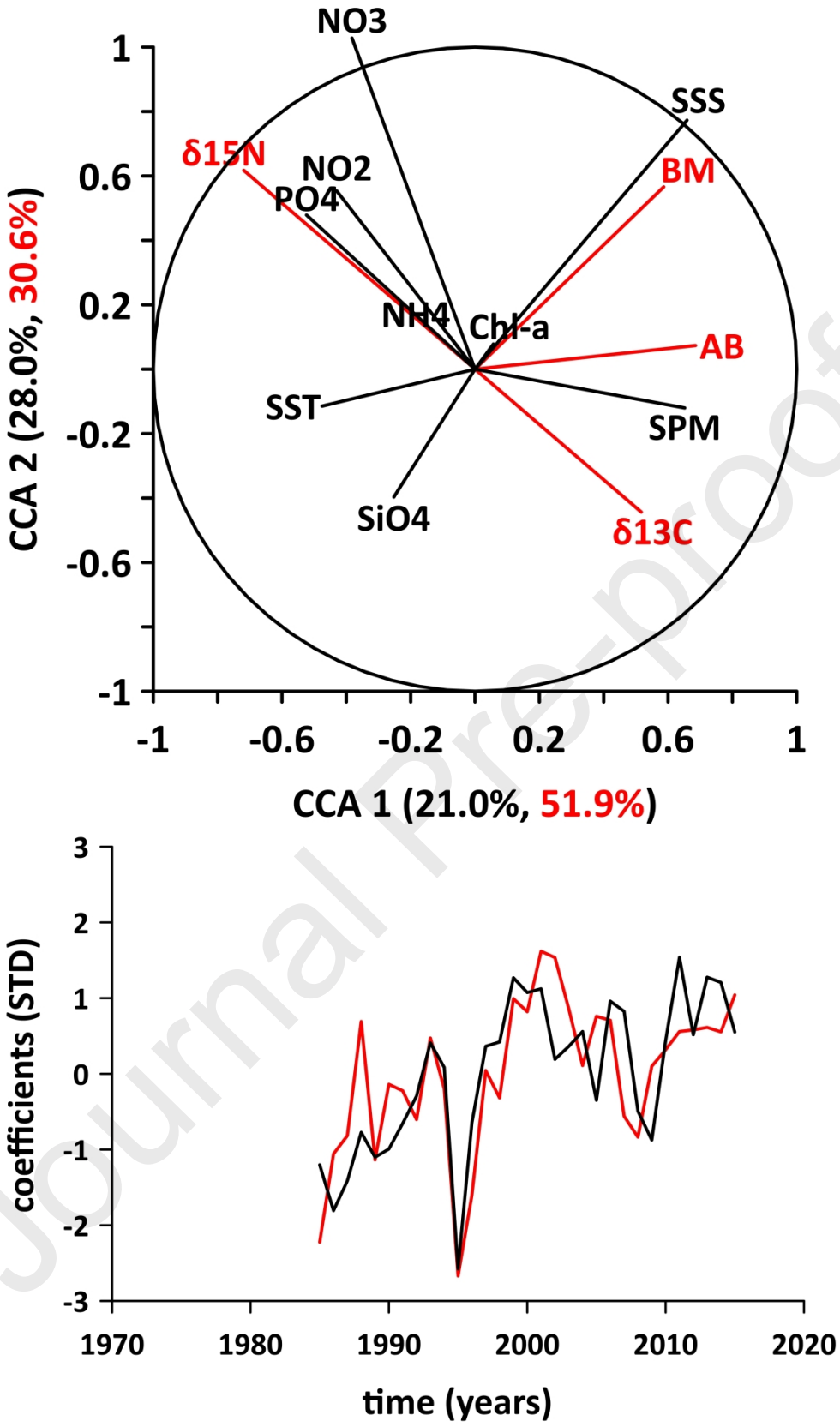

Figure 6e: Explanation see Figure 6a. The predictor–predictand combination is Norderney monitoring–*F. fabula*

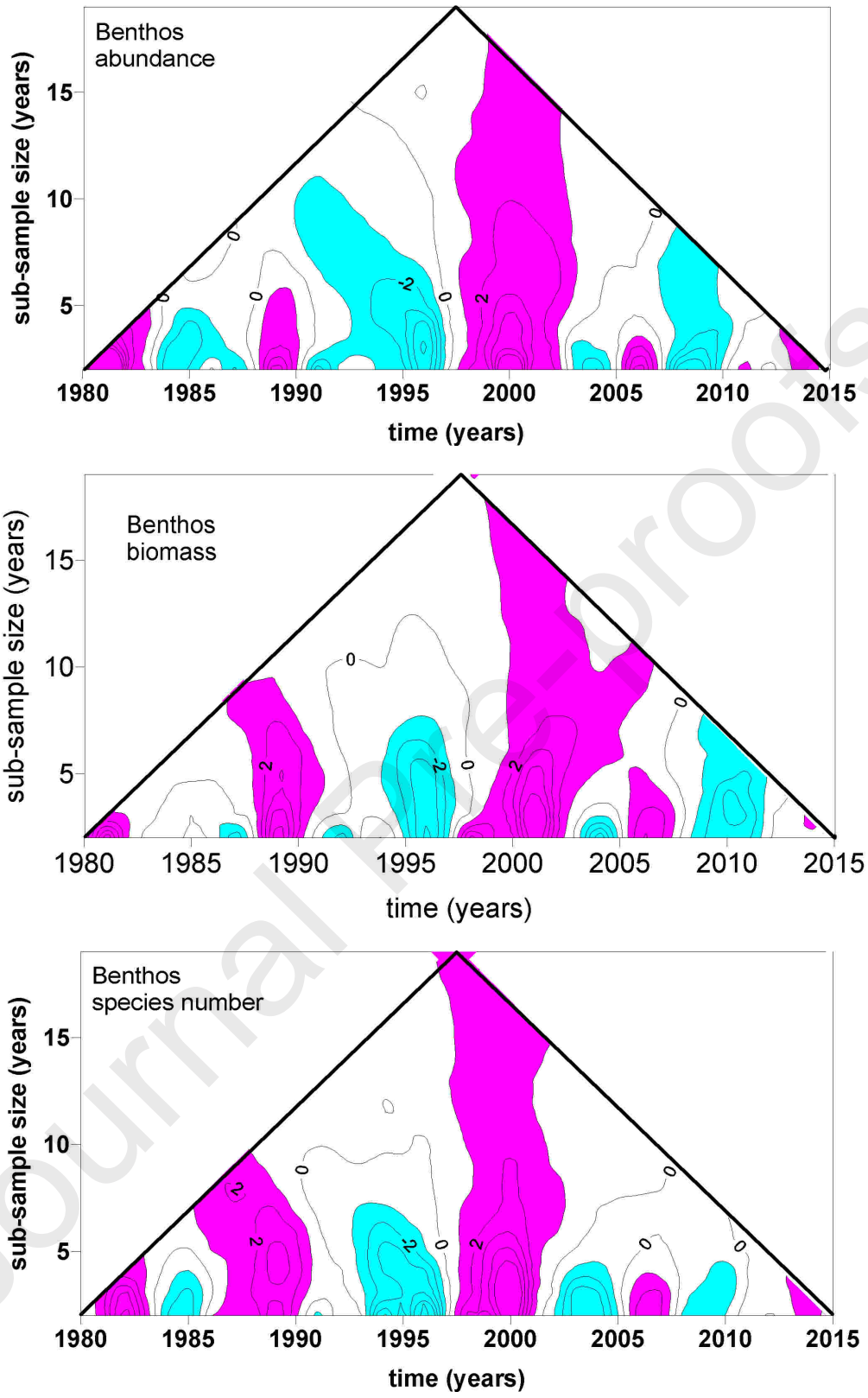

Figure 7: Scanning *t*-test of the benthos time series for abundance, biomass, and species number. Significant changes are shown in color, negative values in cyan and positive values in magenta.

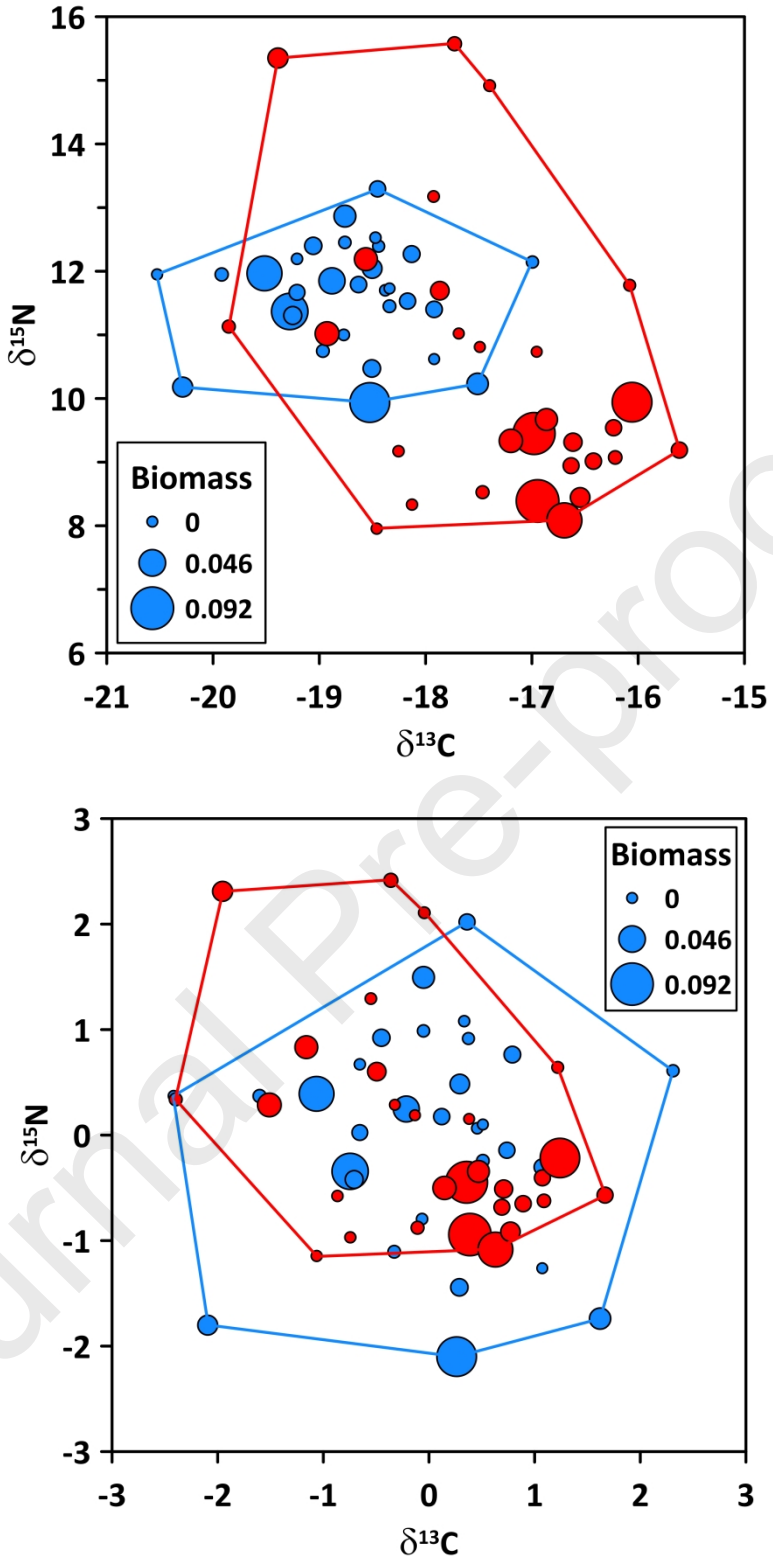

Figure 8: Stable isotope bi-plot showing the means of the corrected carbon and nitrogen isotope values (upper panel) and their standardized values (lower panel), the corresponding convex hulls, and the relative biomass of *Magelona* spp. (blue) and *F. fabula* (red).

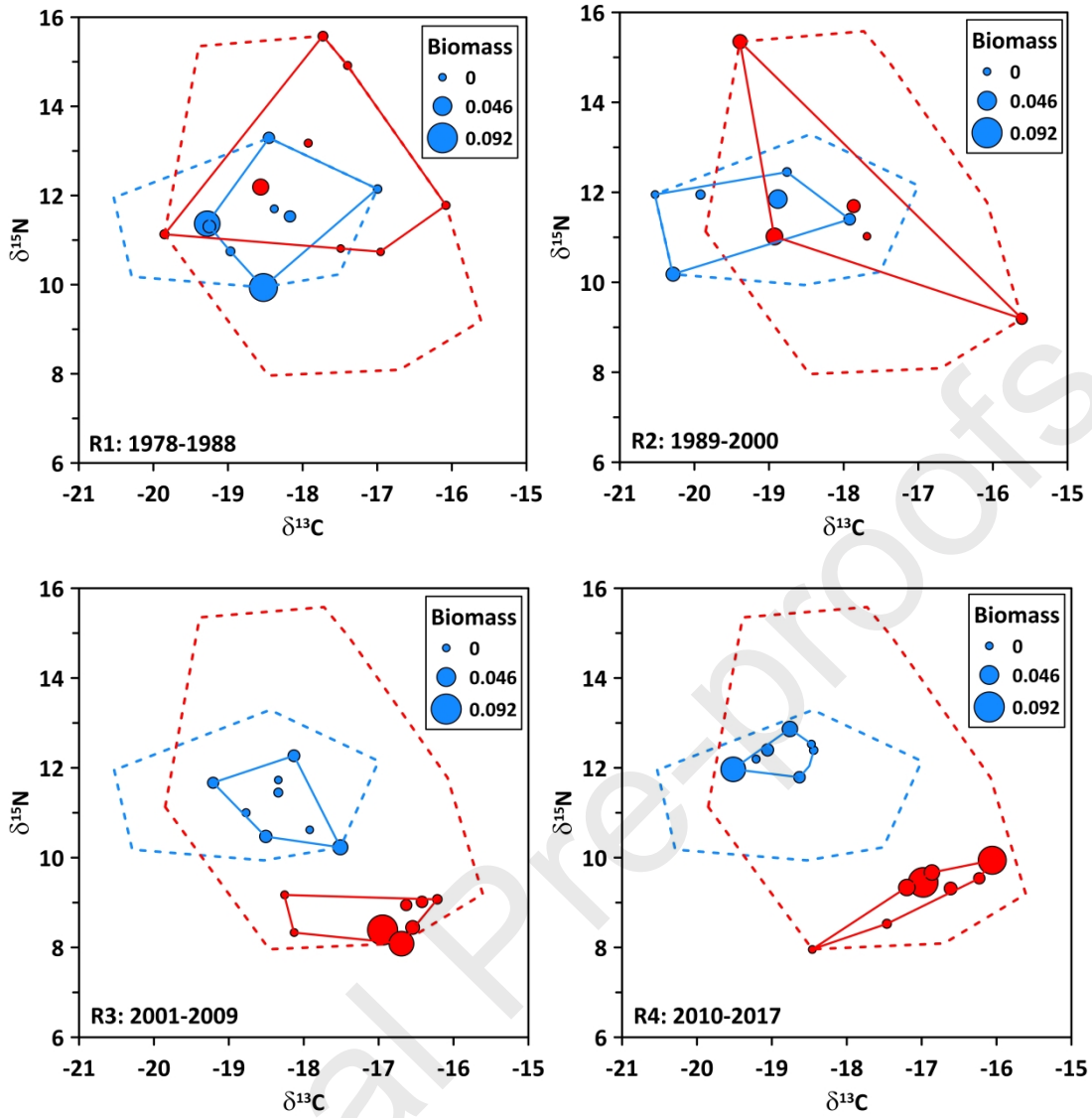

Figure 9: Convex hull and relative biomass of *Magelona* spp. (blue) and *F. fabula* (red) for the four identified regimes (R1–R4) compared with the 40-year data ensemble shown in Figure 8 (dashed lines).

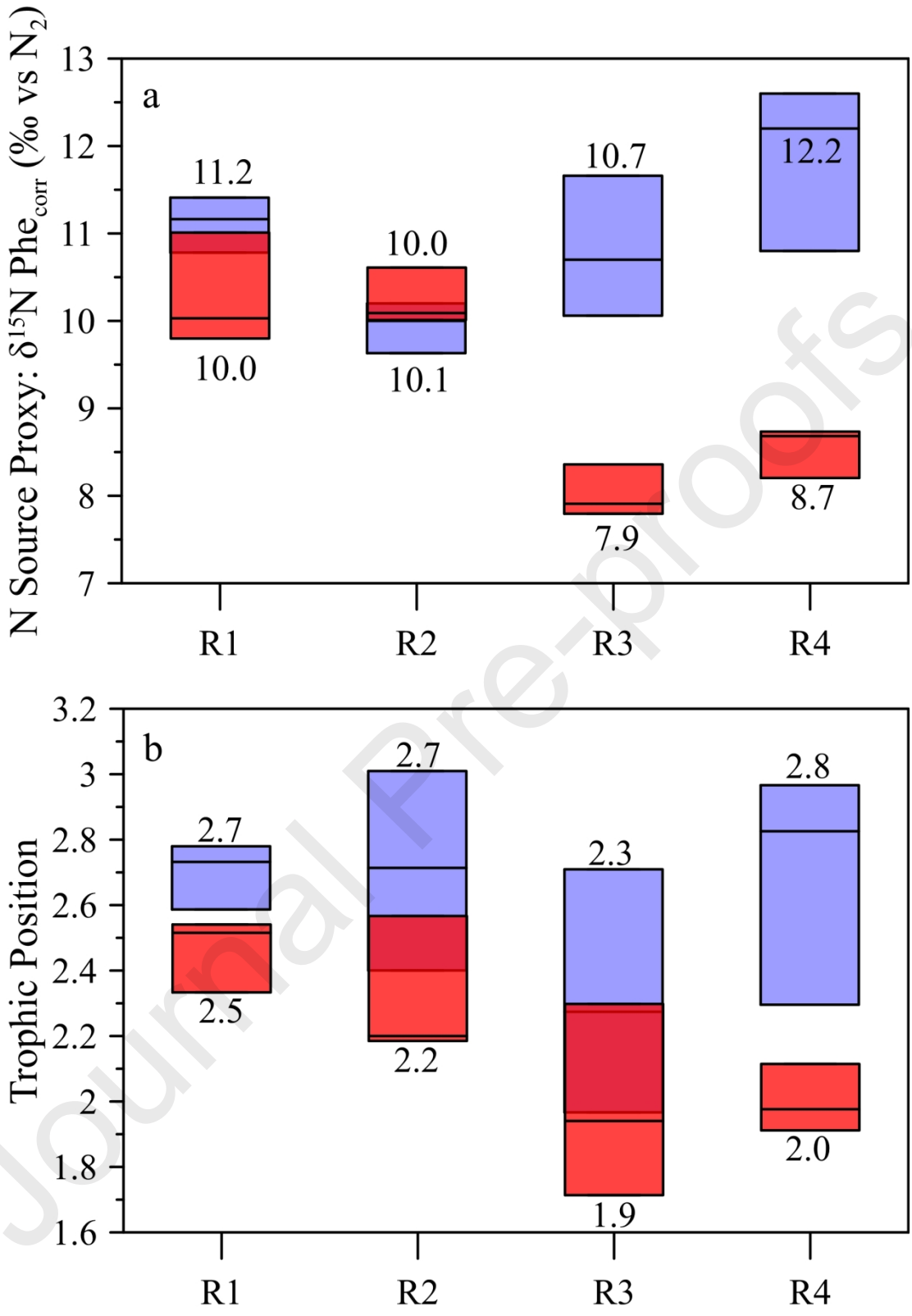

Figure 10: Regime-specific a) stable nitrogen isotope distribution of the N source proxy phenylalanine corrected according to Table 1 ($\delta^{15}N$ Phe_{corr} in ‰ vs. N_2); b) trophic position of *Magelona* spp. (blue) and *F. fabula* (red). N=3 for each box whisker plot. Numbers are the median values.

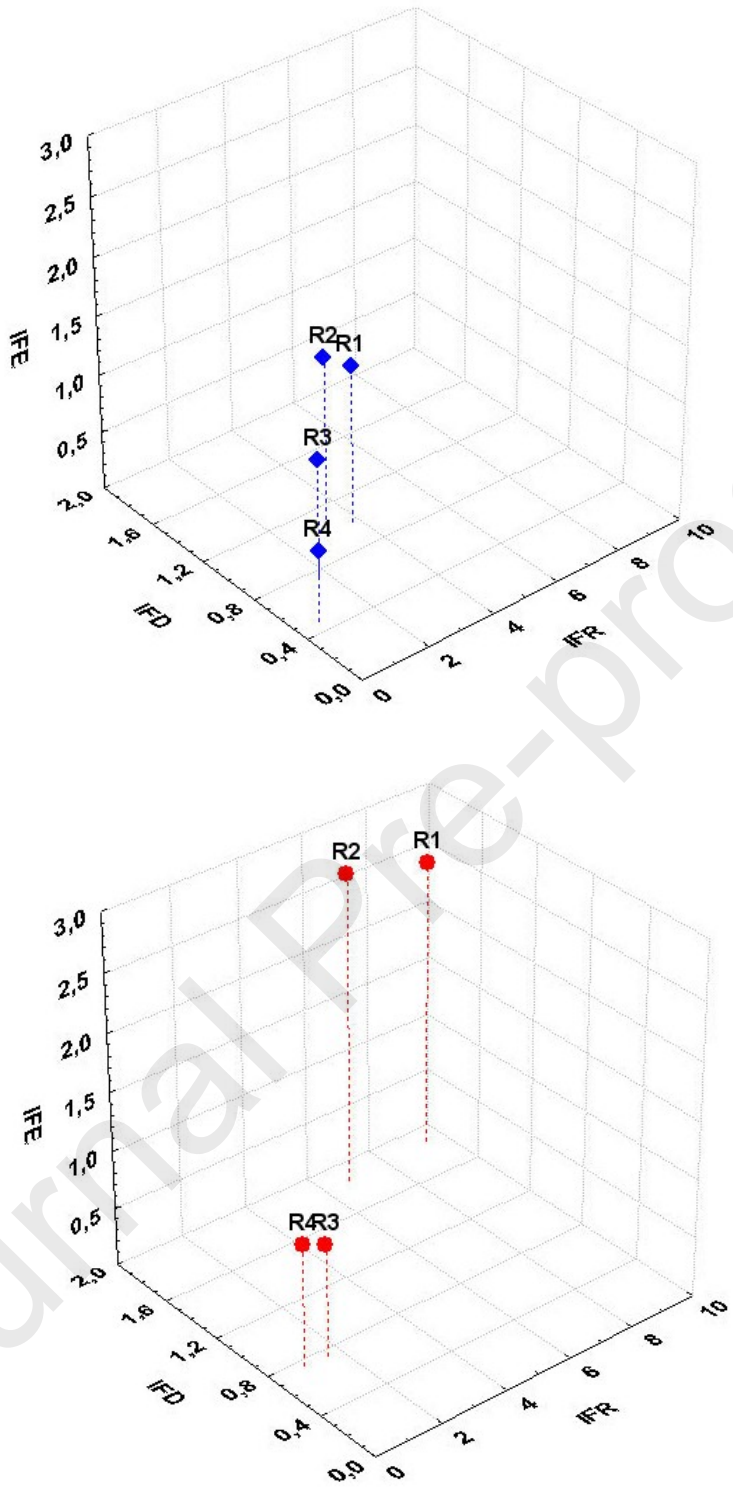

Figure 11: Functional diversity in the four identified regimes for *Magelona* spp. (upper panel) and *F. fabula (*lower panel) in the isotopic functional diversity space constructed from IFR, IFD, and IFE based on the results of the Layman model.

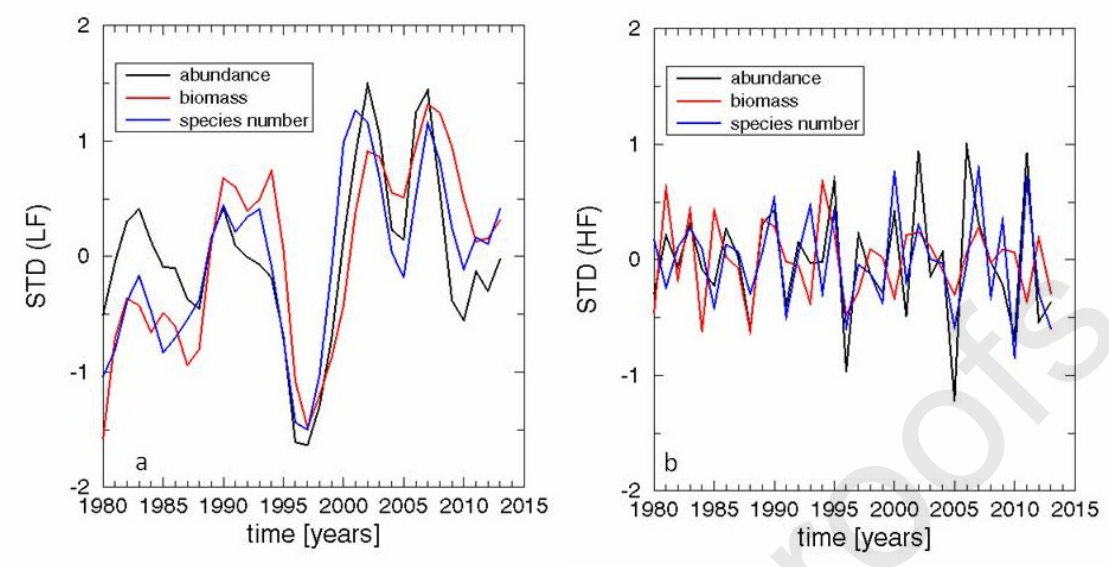

Figure 12: Low-frequency (LF) and high-frequency (HF) benthic time series. LF time series (a) were obtained by low-pass filtering using a cutoff period of 5 years, and HF time series (b) by subtracting the LF time series from the time series itself. The LF part was equivalent to the identified regimes and the trendless HF part to the 3-year memory of the system.

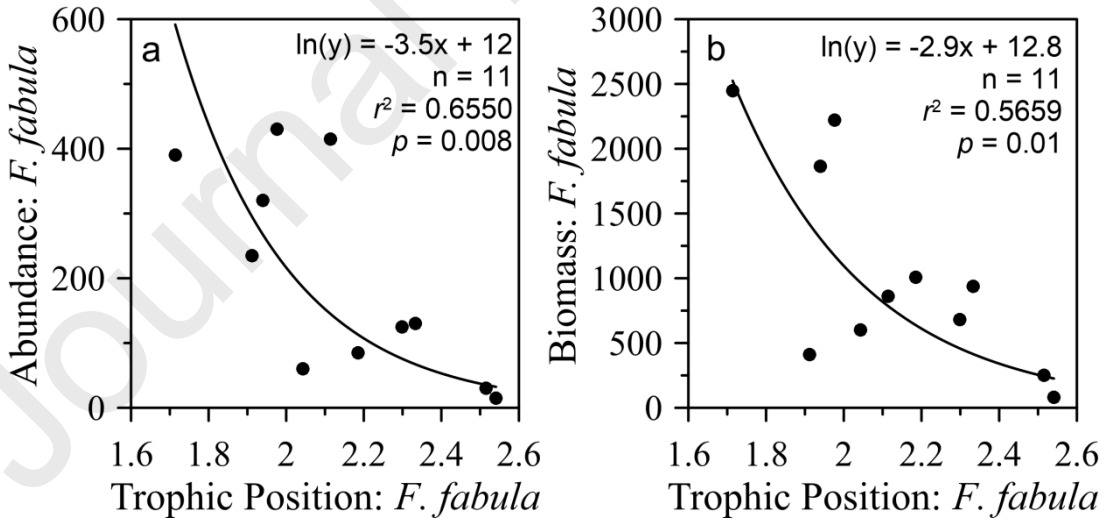

Figure 13: Composite relationships between (a) abundance and (b) biomass vs. the trophic position of *F. fabula*. The exponential regression lines indicate significant relationships between the variables (see the regression equations in the panels).